

Why Transformers Need Adam: A Hessian Perspective

Yushun Zhang ^{*1,2}, Congliang Chen ^{+1,2}, Tian Ding^{‡2}, Ziniu Li^{§1,2},
 Ruoyu Sun^{#1,2}, and Zhi-Quan Luo^{◇1,2}

¹The Chinese University of Hong Kong, Shenzhen, China

²Shenzhen Research Institute of Big Data

Abstract

SGD performs worse than Adam by a significant margin on Transformers, but the reason remains unclear. In this work, we provide an explanation of SGD’s failure on Transformers through the lens of Hessian: (i) Transformers are “heterogeneous”: the Hessian spectrum across parameter blocks vary dramatically, a phenomenon we call “block heterogeneity”; (ii) Heterogeneity hampers SGD: SGD performs badly on problems with block heterogeneity. To validate that heterogeneity hampers SGD, we check various Transformers, CNNs, MLPs, and quadratic problems, and find that SGD works well on problems without block heterogeneity but performs badly when the heterogeneity exists. Our initial theoretical analysis indicates that SGD fails because it applies one single learning rate for all blocks, which cannot handle the heterogeneity among blocks. The failure could be rescued if we could assign different learning rates across blocks, as designed in Adam.

1 Introduction

Transformers [Vaswani et al., 2017] have become a major workhorse behind much remarkable progress in AI development (e.g., [Achiam et al., 2023]). However, the understanding of Transformer training remains limited. For instance, Transformer training largely relies on Adam(W) [Kingma and Ba, 2014, Loshchilov and Hutter, 2017]. In contrast, Stochastic Gradient Descent with momentum (SGD) ¹, which is the de-facto optimizer for convolution neural networks [LeCun et al., 1998] (CNNs), performs poorly on Transformers (see Figure 10 and 11 in Appendix D as evidence). Yet, the cause of failure remains unclear. It is an intriguing question why SGD fails on Transformers. **First**, from a theoretical perspective, this topic helps reveal more properties of the Transformer training loss landscape, which helps boost understanding of training objectives and current optimizers. **Second**, from a computational perspective, Adam requires heavier memory storage than SGD. Compared with SGD, Adam needs to store an additional second-order momentum, which takes at least the same memory of the model size. The memory consumption of Adam has become a major overhead in large-scale transformer training [Rasley et al., 2020]. Identifying the cause of failure may help researchers design more efficient optimizers.

In this work, we explore the failure mode of SGD through the lens of Hessian. We start by investigating the *full* Hessian spectrum of Transformers, i.e., the full eigenvalue density of Hessian (see Figure 1 as

*Email: yushunzhang@link.cuhk.edu.cn. Our code is available at <https://github.com/zyushun/hessian-spectrum>.

+Email: congliangchen@link.cuhk.edu.cn

‡Email: dingtian@sribd.cn

§Email: ziniu.li@link.cuhk.edu.cn

#Correspondence author. Email: sunruoyu@cuhk.edu.cn

◇Email: luozq@cuhk.edu.cn

¹We introduce the update rules of Adam(W) and SGD in Appendix B.1.

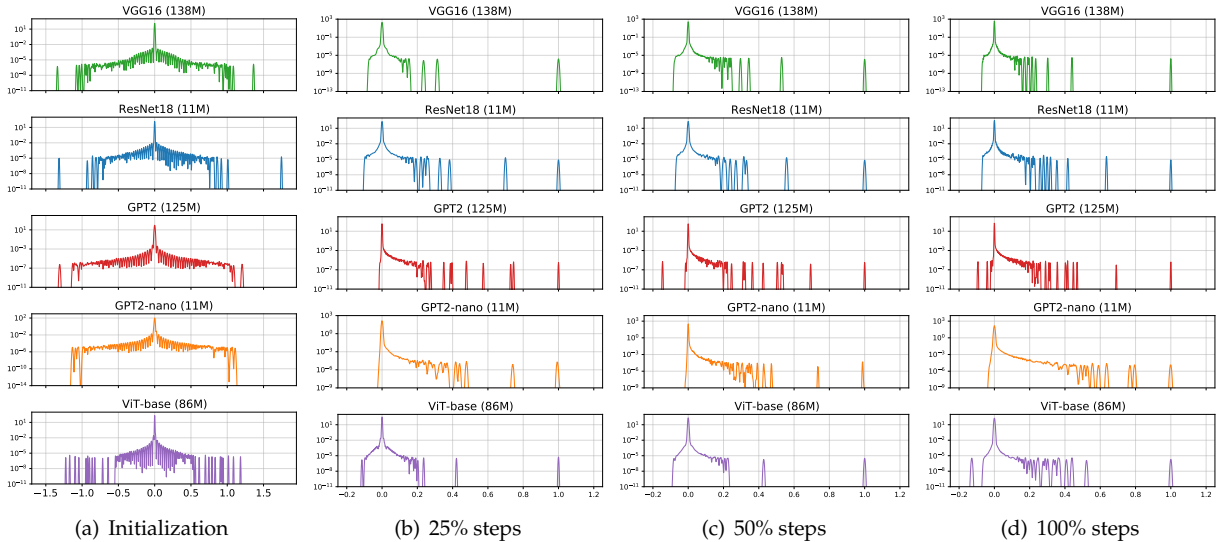


Figure 1: The full Hessian spectra of CNNs (VGG16 and ResNet18) and Transformers (GPT2, GPT2-nano, and ViT-base) at different training stages. The x -axis records the eigenvalues and the y -axis records the frequency in the log scale. To allow comparison in the same figure, the plotted spectra are normalized by their 10-th largest eigenvalues. We find that the spectra on CNNs and Transformers are largely similar.

an example). By theory, the full Hessian spectrum largely determines the behavior of gradient methods [Nesterov, 2013, Goh, 2017, Sun, 2019, Goujaud et al., 2022], so we suspect it can also help uncover the reasons behind SGD failure on Transformers. Using numerical linear algebra tools [Bai et al., 1996], we empirically compare the full spectra of CNNs (the scenarios where SGD is on par with Adam) and those of Transformers (where SGD largely lags behind Adam). Unfortunately, in Figure 1, we find that the spectra on CNNs and Transformers are often largely *similar* despite the different optimizer behaviors on these tasks. As such, we have *not* identified critical phenomena in the full Hessian spectra associated with SGD’s failure on Transformers. To reveal the cause of failure, we need a more fine-grained investigation into Hessian.

What else could make SGD fail on Transformers, but not on CNNs? By dissecting the structures of CNNs and Transformers, we observe that CNN architectures are constructed by the repetitive stacking of *similar* parameter blocks (convolution layers), while Transformers involve the interleaved stacking of *disparate* parameter blocks (e.g. Query, Key, Value blocks in attention and MLP layers). We suspect that these design differences may lead to different properties in optimization. Intuitively, disparate parameter blocks would contribute differently to the total loss. So each block might prefer a distinct treatment by optimizers, which can be provided by Adam but not by SGD. This motivates us to investigate the Hessian spectrum of each parameter block, abbreviated as the blockwise Hessian spectrum.

By inspecting the blockwise Hessian spectrum, we find a possible explanation why SGD fails on Transformers. We find that Transformers are “heterogeneous”: for all Transformers we checked, Hessian spectra of different parameter blocks are dramatically different. We then verify that such heterogeneity indeed hampers SGD via extensive experiments on various Transformers, CNNs, MLPs, and quadratic problems. Our contributions are summarized as follows.

- **Exploring the failure mode of SGD on transformers.** We provide an explanation why SGD largely lags behind Adam on Transformers through the lens of blockwise Hessian spectrum. This explanation consists of two parts. First, we identify a phenomenon called “block heterogeneity”, which states that Hessian spectra are dramatically different across parameter blocks. We find this phenomenon prevalent on all Transformers in our experiments, but *not* on CNNs. Second, we verify that block heterogeneity hampers SGD. More specifically, on various kinds of Transformers, CNNs, MLPs, we

find that SGD always performs badly on problems with block heterogeneity but works well otherwise.

- **Theoretical results on quadratic models.** We build various convex quadratic problems, some with block heterogeneity and others without block heterogeneity. We find that GD is significantly worse than Adam on problems with block heterogeneity, but performs similarly to Adam otherwise. We provide a theoretical result which shows that GD indeed works badly on quadratic problems with block heterogeneity. Our analysis suggests that one important reason for (S)GD failure is that it uses one single learning rate for all blocks, which cannot handle the heterogeneity among blocks. The failure could be saved if we assign different learning rates across blocks like Adam.

2 Main Results

2.1 Problem Settings

Notations. We denote the full-batch training loss as $\mathcal{L}(w) \equiv \frac{1}{n} \sum_{i=1}^n \mathcal{L}_i(w)$, where n is the number of minibatches, $\mathcal{L}_i(w)$ is the loss of i -th minibatch and $w \in \mathbb{R}^d$ is the neural network parameters. We denote the gradient and Hessian of the training loss w.r.t. neural network parameters as $\nabla \mathcal{L}(w) \in \mathbb{R}^d$ and $\nabla^2 \mathcal{L}(w) \in \mathbb{R}^{d \times d}$, respectively. We use $\nabla \mathcal{L}_i(w) \in \mathbb{R}^d$ and $\nabla^2 \mathcal{L}_i(w) \in \mathbb{R}^{d \times d}$ to denote the i -th minibatch counterparts. We use $[d]$ to denote the index set $\{1, 2, \dots, d\}$. Given an arbitrary partition $\{\mathcal{D}_l\}_{l=1}^L$ over $[d]$ with $d_l \triangleq |\mathcal{D}_l|$, we can split w into L parameter blocks $\{w_l\}_{l=1}^L$, where $w_l = \mathbb{R}^{d_l}$ consists of parameters with indexes in the l -th block \mathcal{D}_l . We denote $[\nabla^2 \mathcal{L}(w)]_l \in \mathbb{R}^{d_l \times d_l}$ as the Hessian of l -th parameter-block w_l , where $[\nabla^2 \mathcal{L}(w)]_{l,i,j} = \frac{\partial^2}{\partial w_{l,i} \partial w_{l,j}} \mathcal{L}(w_l)$. Note that $[\nabla^2 \mathcal{L}(w)]_l$ is the l -th principle block sub-matrix of $\nabla^2 \mathcal{L}(w)$.

Preliminaries. Hessian of large-scale NNs are intractable to obtain due to the numerical difficulties of computing and storing them. Fortunately, there are extensive numerical linear algebra methods to approximate the Hessian spectrum without calculating the Hessian explicitly. Among which, the Stochastic Lanczos Quadrature method (SLQ) [Bai et al., 1996] is known to be one of the oldest yet the most powerful methods. SLQ is a combination of the stochastic trace estimator [Hutchinson, 1989], the Gaussian quadrature [Golub and Meurant, 2009, Epperson, 2013], and the Lanczos algorithm [Lanczos, 1950]. In short, SLQ takes a handful of Hessian-vector products as input, where the vectors are sampled from the normalized Rademacher distribution. It returns a smooth curve on \mathbb{R} that approximates the histograms of eigenvalues (see Figure 1 as an example). Since the derivation of SLQ is quite involved, we defer the detailed description of SLQ to Appendix B.2. The algorithmic form of SLQ can be seen in Algorithm 5 in the Appendix. We provide running time analysis and detailed setup of SLQ in Appendix C.1.

In this work, we apply SLQ to various CNNs and Transformers on different datasets. As for CNNs, we study CNNs including ResNet18 (11M) and VGG16 (138M) on ImageNet [He et al., 2016, Simonyan and Zisserman, 2014]. As for Transformers, we study ViT-base (86M) on ImageNet [Dosovitskiy et al., 2020], BERT (40M) on Cornell Movie-Dialogs Corpus [Devlin et al., 2018], and GPT2 (125M) on Openwebtext [Radford et al., 2019]. For a fair comparison with ResNet18, we also consider smaller models like GPT2-nano² (11M) on English corpus. The largest model we conduct is GPT2 with 125 million parameters. Detailed experimental setups are shown in Appendix C.1. For all these Transformer-based tasks, SGD performs significantly worse than Adam; while for CNN-based takes, Adam and SGD are similar. The performance comparison is shown in Figure 10 and 11 in the Appendix. We estimate the spectrum of (1) the full Hessian $\nabla^2 \mathcal{L}(w)$ and (2) the Hessian of all parameter blocks $[\nabla^2 \mathcal{L}(w)]_l, l \in [L]$. For (2), we split w according to the default partition in PyTorch implementation, e.g., Embedding layer, Query in 1st attention layer, Key in 1st attention layer, Value in 1st attention layer, etc..

Note that the term "block" is a bit different from the term "layer". For instance, Query and Key could be in the same layer, but they are different parameter blocks. In the following contexts, we refer to "full

²<https://github.com/karpathy/nanoGPT/>

Hessian spectrum" as the estimated spectrum of $\nabla^2\mathcal{L}(w)$ and "blockwise Hessian spectrum" as the estimated spectrum of $[\nabla^2\mathcal{L}(w)]_l, l \in [L]$.

2.2 Full Hessian Spectrum Is Not Informative Enough

Motivated by classical theory, we start by investigating the full Hessian spectrum of Transformers. We choose to study the full Hessian spectrum for two reasons. First, as mentioned in Section 1, the full Hessian spectrum is known to largely determine the behavior of gradient methods. For instance, the range of the spectrum will affect the convergence rate [Nesterov, 2013]. Second, the full Hessian spectrum has been shown to be informative in explaining multiple phenomena in neural nets (NNs), e.g., how BatchNorm accelerates the training [Ghorbani et al., 2019]. Due to these reasons, we hypothesize that the full Hessian spectrum can also help uncover the reasons behind SGD failure on Transformers.

We compare the full spectra of CNNs (the scenarios where SGD is on par with Adam) and those of Transformers (where SGD largely lags behind Adam). The results are shown in Figure 1. Unfortunately, our experiments show that the full Hessian spectrum might *not* be enough to explain the SGD failure on Transformers. We explain as follows. The primary information of the spectrum lies in its (1) dispersion, (2) shape, and (3) evolution along training. As for (1), we find that eigenvalues are dispersed very similarly and we do not observe any notably large eigenvalues in the spectra of Transformers. So (1) does not seem to be related to the failure of SGD. We further inspect (2) and (3). For all CNNs and Transformers in Figure 1, we find similar phenomena: the shape of the spectrum is approximately symmetrical around 0 at initialization. As training proceeds, the majority of large negative eigenvalues disappear and the shape evolves into a combination of a "bulk" and some "outliers". Since the spectral shape and evolution are quite similar on Transformers and CNNs, they cannot explain the failure of SGD on Transformers, either. In summary, we have not identified critical phenomena in the full Hessian spectra linked to SGD's failure on Transformers.

2.3 Main Findings Through Blockwise Hessian Spectra

We have shown that the full Hessian spectrum seems not sufficient for uncovering the reason why SGD fails on Transformers. What else could make SGD fail on Transformers, but not on CNNs? We find two important features that are overlooked in the full Hessian spectrum analysis above.

- **(1)** The Hessian structure is overlooked. There are numerical results showing that the Hessians are close to *block-diagonal matrices* on MLPs [Collobert, 2004, Roux et al., 2007, Martens and Grosse, 2015]. We restate their findings in Appendix C.2. Further, [Collobert, 2004, Section 7] theoretically shows that the block diagonal structure comes from (i) the layer-by-layer design in NNs and (ii) the Cross-Entropy loss. Following this line of work, we also observe a near block-diagonal Hessian in small Transformers in Figure 2, where the variables in each principle block correspond to the parameters of each block in the Transformer. These results suggest that near block-diagonal Hessian might be common in NNs.
- **(2)** The build-up rules of Transformers is overlooked. Transformers are built upon stacking of *disparate* parameter blocks, e.g. Query, Key, Value blocks in attention, and MLP layers. This is largely different from CNNs, which are constructed by the repetitive stacking of *similar* parameter blocks (convolution layers). Since each parameter blocks in Transformers are designed differently, they might have different properties for optimization, which might further affect the optimizer behavior.

Combining **(1)** and **(2)**, we hypothesize that the blockwise Hessian spectrum might provide some insights on distinguishing CNNs and Transformers. What extra information can be contained in the blockwise spectrum but not in the full spectrum? By definition, the blockwise Hessians form the principal block sub-matrix of the full Hessian. For block diagonal matrices, blockwise Hessian encodes the location of eigenvalues, i.e., which block does an eigenvalue (of the full Hessian) lie in, while the full spectrum ignores this. In the following, we study blockwise Hessian spectra on various models. We will show that blockwise spectra indeed carry more information than the full spectrum for distinguishing CNNs and Transformers.

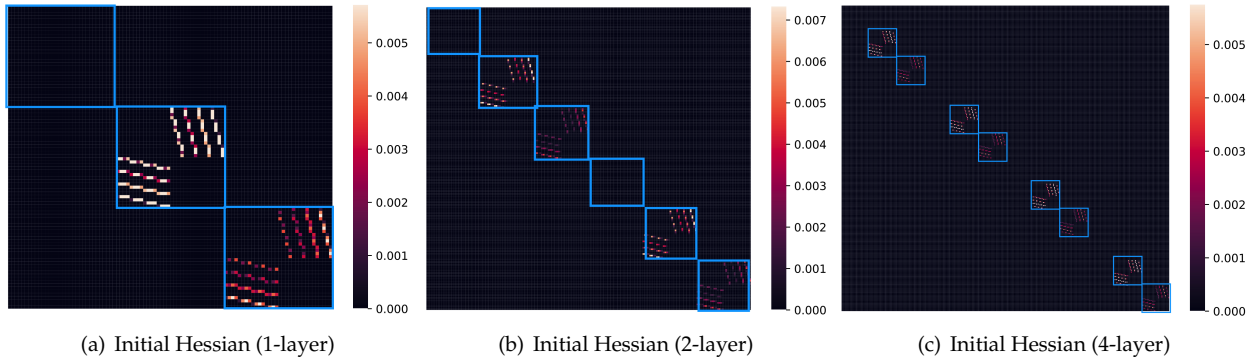


Figure 2: The initial Hessian of small Transformers with 1, 2, and 4 layers on a subset of Openwebtext. We take the absolute value of each entry to distinguish non-zero values (including negatives) from those near 0. See implementation details in Appendix C.2. We observe a near block-diagonal structure in Hessian.

We here demonstrate the shape of blockwise spectra in CNNs and Transformers. We sample four blocks per model and present the spectra in Figure 3. In Transformers, the Hessian spectra of embedding, attention, and MLP blocks are largely *different*. In contrast, in CNNs, the spectra of convolution layers are *similar*. We further verify this observation for the rest of the parameter blocks. We calculate the Jensen-Shannon (JS) distance between two eigenvalue densities of all possible block pairs. We show the results in Figure 4.

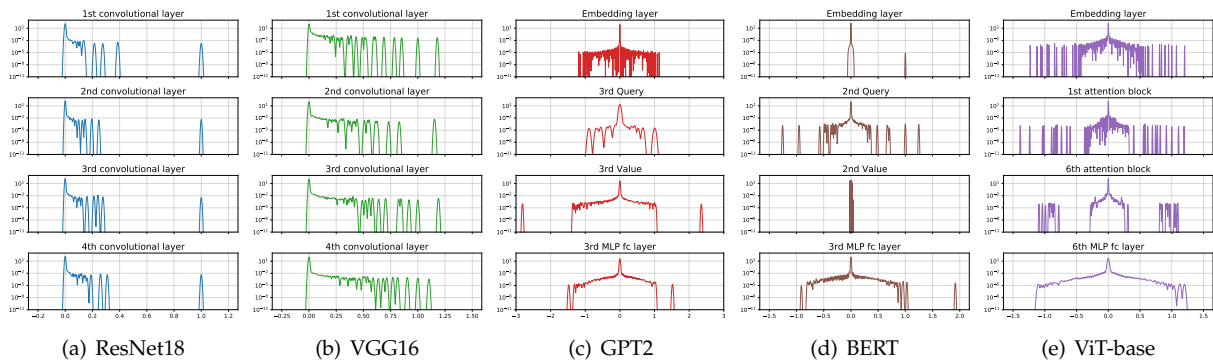


Figure 3: The blockwise Hessian spectra of CNNs (ResNet18 and VGG16) and Transformers (GPT2, BERT, and ViT-base) at initialization. The x -axis records the eigenvalues and the y -axis records the frequency in the log scale. To allow comparison in the same figure, we here only present the spectra of 4 blocks in each model. The plotted spectra are normalized by their 10-th largest eigenvalues. We find that the spectra in CNNs are similar among blocks, while the spectra in Transformers are different across blocks.

The results in Figure 4 showed an interesting phenomenon: for all the Transformers we checked, the blockwise Hessian spectra are largely *different* across blocks. In the following, we refer to this phenomenon as “**block heterogeneity**”. As a control group experiment, the blockwise Hessian spectra of CNNs are *similar* and the block heterogeneity is *not* observed. We refer to this phenomenon as “**block homogeneity**”. These results indicate that block heterogeneity is informative in distinguishing CNNs and Transformers. Intuitively, the block-homogeneous Hessian in a CNN comes from the repetitively similar convolution layers, while the block-heterogeneous Hessian in a Transformer stems from the interleaved stacking disparate layers such as Query, Value, and MLPs. In the following, we will show that the block heterogeneity is strongly correlated with the failure of SGD on Transformers.

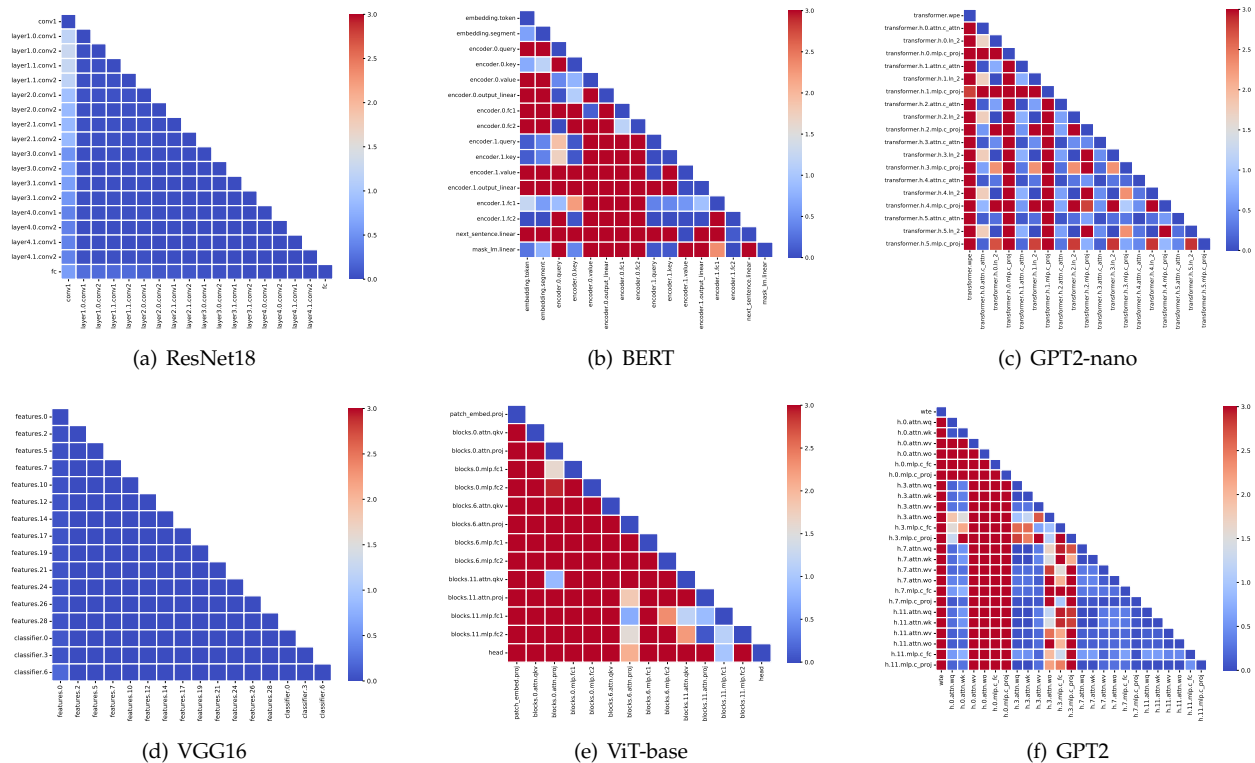


Figure 4: The JS distance among blockwise Hessian spectra for different models at initialization. We find that the JS distance of blockwise spectra in CNNs is significantly smaller than that in Transformers.

2.4 SGD Fails on Simple MLPs with Block Heterogeneity

We now further link block heterogeneity to the failure of SGD. We construct a simple example without attention layers but has block heterogeneity and find that SGD still fails. We consider a 4-layer MLP on MNIST. Using standard MLP, we find that the Hessian exhibits a homogeneous block structure and SGD converges as fast as Adam. We then scale the output of each layer by a constant c . We define c as the degree of heterogeneity since larger c would bring more heterogeneity to the Hessian (see Table 3 in the Appendix). As shown in Figure 5, we find that the gap between Adam and SGD increases with the degree of heterogeneity. This example shows that attention might not be the root cause of SGD failure, but the block heterogeneity (brought by attention) might be.

2.5 Implication on Choosing SGD or Adam

The above findings could bring up an interesting empirical guidance: we can compute the blockwise spectrum of initial Hessian, and then decide whether to use Adam or SGD. Such a method could be useful in scenarios in training large models that are not mainstream Transformers or CNNs, e.g., Mamba [Gu and Dao, 2023]. In these cases, there is not much prior experience in choosing optimizers. It would be intriguing to decide whether SGD is suitable for the task before the training is launched. We present two reasons.

- In large-scale model training, memory is limited but the model size grows, so Adam could become a major computational burden due to the memory of 2nd-order momentum (as mentioned in Section 1 and [Rasley et al., 2020]).

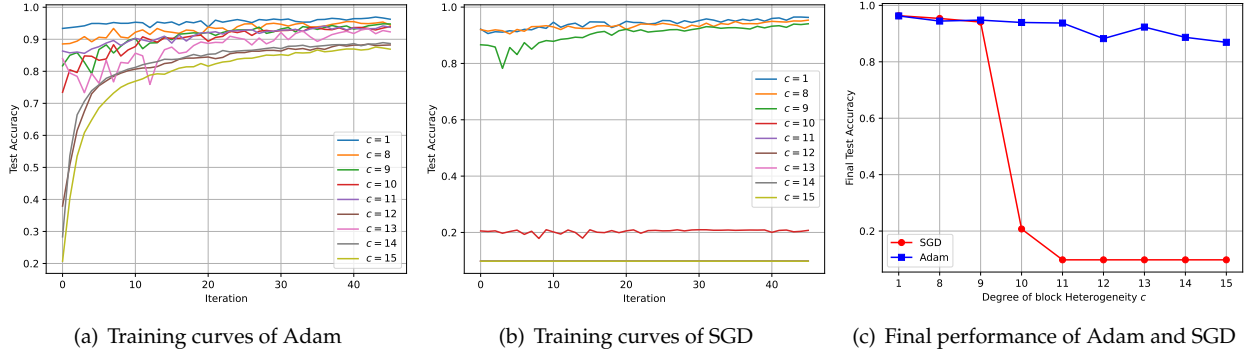


Figure 5: The performance of SGD and Adam on MNIST with 4-layer MLPs under different degrees of block heterogeneity c . In (c), each point records the best-converged test accuracy under the learning rate grid search. See more details in Appendix C.3. We observe that SGD performs worse as heterogeneity increases.

- SGD is a lightweight alternative to Adam, but the performance of SGD may be bad. In large NN training, it might take days (or even weeks) to obtain informative feedback from training logs, so it is expensive to conduct trial and error to choose an appropriate optimizer. Specifically, if SGD performs badly, it would be difficult to judge whether the bad performance is due to improper learning rates or other more fundamental reasons. Then, it would be hard to decide whether to switch the optimizer.

Motivated by the above reasons, we here propose a quantitative metric that could predict the failure of SGD before the training is launched. With the help of this metric, we could save much expense on the trial and error for SGD. The metric is simply the averaged JS distance among blockwise Hessian spectra at initialization, i.e., the averaged value in each heatmap of Figure 4. We denote it as JS^0 . We present JS^0 of various models in Table 1. We note that JS^0 establishes a quantitative difference between the loss landscape of Transformers and CNNs. As argued in the previous sections, this quantity can predict the failure of SGD. Note that JS^0 is independent of optimizers and could be efficiently checked in priori before training.

Model	ResNet18	VGG16	ViT-base	BERT	GPT2-nano	GPT2
JS^0	0.10	0.09	286.41	53.38	14.93	83.23

Table 1: JS^0 denotes the average JS distance between the initial Hessian spectra of each pair of parameter blocks. We find that the JS^0 on CNNs is at least $140\times$ smaller than on Transformers. JS^0 establishes a quantitative difference between the loss landscape of Transformers and CNNs.

To summarize this section, we provide an explanation for SGD’s failure. We identify a phenomenon called block heterogeneity. This phenomenon naturally exists in Transformers, but not in CNNs. This phenomenon can exist in non-Transformer architectures as well. Our experiments suggest a strong connection between the failure of SGD and block heterogeneity. Our findings could provide empirical guidance to decide whether to use Adam or SGD.

3 Case Study of Quadratic Models and Preliminary Theory

Now we construct quadratic functions with block diagonal Hessian. We will compare the performance of GD and Adam on Hessian with and without block heterogeneity. Initial theoretical results on these quadratic models will be provided. Note that insights on quadratic models could be important for understanding realistic NNs, as mentioned by researchers such as LeCun et al. [2002] and OpenAI team [Kaplan et al., 2020].

3.1 Settings and Additional Notations

We consider $\min_w \mathcal{L}(w) = \frac{1}{2}w^T H w - h^T w$ where $H \in \mathbb{R}^{d \times d}$ is positive definite and $h \in \mathbb{R}^d$. We denote \mathcal{L}^* as the minimum value of $\mathcal{L}(w)$. We set H as a block diagonal matrix: $H = \text{diag}(H_1, \dots, H_L)$, where $H_l \in \mathbb{R}^{d_l \times d_l}$ and $d = \sum_{l=1}^L d_l$. We use $w_l \in \mathbb{R}^{d_l}$ to denote the variable in the l -th block and $w = (w_1^T, \dots, w_L^T)^T \in \mathbb{R}^d$. Similarly for $h_l \in \mathbb{R}^{d_l}$. Similarly, we use $[\nabla \mathcal{L}(w)]_l \in \mathbb{R}^{d_l}$ to denote the gradient in the l -th block and denote $[\mathcal{L}(w)]_l = \frac{1}{2}(w_l^T)^T H_l w_l^t - h_l^T w_l$ as the objective function w.r.t. the l -th block. Note that $\mathcal{L}(w) = \sum_{l=1}^L [\mathcal{L}(w)]_l$. We denote $\lambda_1 \geq \lambda_2 \geq \dots \geq \lambda_d$ as the eigenvalues of H . Similarly for $\lambda_{l,1} \geq \dots \geq \lambda_{l,d_l}$. We denote $\kappa = \frac{\lambda_1}{\lambda_d}$ and $\kappa_l = \frac{\lambda_{l,1}}{\lambda_{l,d_l}}$ as the condition number of H and H_l , respectively. We say an algorithm has complexity $\tilde{\mathcal{O}}(C)$ if it takes $\mathcal{O}(C \log(1/\epsilon))$ iterations to achieve error $\frac{\mathcal{L}(w) - \mathcal{L}^*}{\mathcal{L}(w^0) - \mathcal{L}^*} \leq \epsilon$, where w^0 is the initial point.

3.2 Experimental Observations

For all experiments, we choose $h = 0$. We consider four types of Hessian H as follows.

- **Case 1: Hessian with Transformer-type spectra.** We choose $L = 4$ and $d_l = 100$. For $l \in [L]$, we construct $H_l = Q_l \Lambda_l Q_l^T$ where Q_l are independent standard Gaussian random matrix and Λ_l are diagonal matrices. For the diagonal elements in Λ_l , we sample d_l numbers according to the spectrum of the embedding layer; 3rd Query, 3rd Value, 3rd MLP (fc layer) in GPT2. Shifting and proportional scaling are performed to ensure all elements in Λ_l lie in the interval $[1, 2000]$. This ensures strong convexity and controls the condition number of H equals 2000. The spectra of H_l are in Figure 6.
- **Case 2: Hessian with CNN-type spectra.** We consider the same setup as **Case 1**. For the diagonal elements in Λ_l , we sample d_l numbers according to the spectrum of the 1st to 4th convolution layers in ResNet18. We shift and proportionally scale the elements Λ_l to the interval $[1, 2000]$ to ensure the strong convexity and the condition number H equals 2000. The spectra of H_l are shown in Figure 7.
- **Case 3: Hessian with simplified heterogeneous spectra.** We choose $L = 3$ and $d_l = 3$. For $l \in [L]$, we construct $H_l = Q_l \Lambda_l Q_l^T$ where Q_l are independent standard Gaussian random matrix and Λ_l are diagonal matrices. We set the diagonal elements of Λ_l as $\{1, 2, 3\}$, $\{99, 100, 101\}$, $\{1998, 1999, 2000\}$ for $l = 1, 2, 3$, respectively. The spectra of H_l are different due to their different supports. The condition number of Hessian H is 2000.
- **Case 4: Hessian with simplified homogeneous spectra.** We consider the same setup as **Case 3**. We set the diagonal elements of Λ_l as $\{1, 99, 1998\}$, $\{2, 100, 1999\}$, $\{3, 101, 2000\}$ for $l = 1, 2, 3$, respectively. The spectra of H_l are similar. The condition number of Hessian H is 2000.

Note that in all four cases, the Hessian share the same condition number. We study two types of optimizers: one that assigns a single learning rate for all blocks, and ones that assign different learning rates across blocks. The optimizers are introduced as follows.

- **Single-learning-rate optimizer.** We study gradient descent (GD).

$$w^{t+1} = w^t - \eta \nabla \mathcal{L}(w) = w^t - \eta(Hw^t - h) \quad (1)$$

We use the optimal learning rate $\eta = \frac{2}{\mu+L}$ [Nesterov, 2013]. We use a standard Gaussian random vector as initialization.

- **Coordinate-wise-learning-rate optimizer.** We study Adam with a constant learning rate and with no bias correction for simplicity (Algorithm 3). We set $\beta_1 = 0$ to erase the effect of momentum. This helps us to focus on the effect of coordinate-wise learning rate (or the effect of diagonal preconditioning) in Adam. We use $\epsilon = 0$. We consider $\beta_2 = 1$ and $\beta_2 = 0.999$, respectively. When $\beta_2 = 1$, Adam assigns

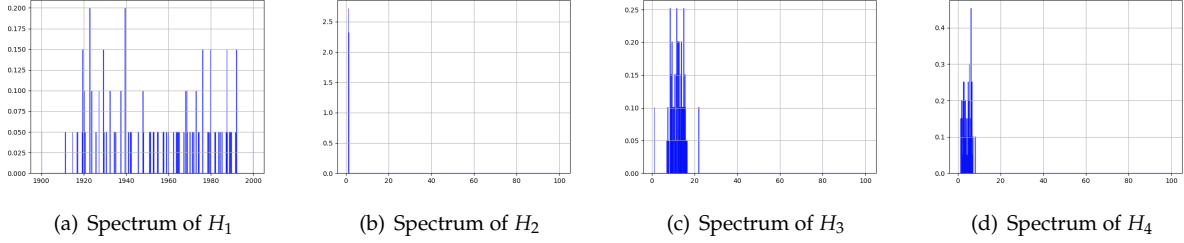


Figure 6: Histogram of eigenvalues of each block in **Case 1** (the heterogeneous case). The eigenvalues in the four blocks are sampled from the spectrum of the embedding layer; 3rd Query, 3rd Value, 3rd MLP (f c layer) in GPT2, respectively. All the eigenvalues are shifted and proportionally scaled such that: the objective function is strong convex; the condition number of Hessian equals 2000; their relative ranges are preserved; and the block heterogeneity is preserved.

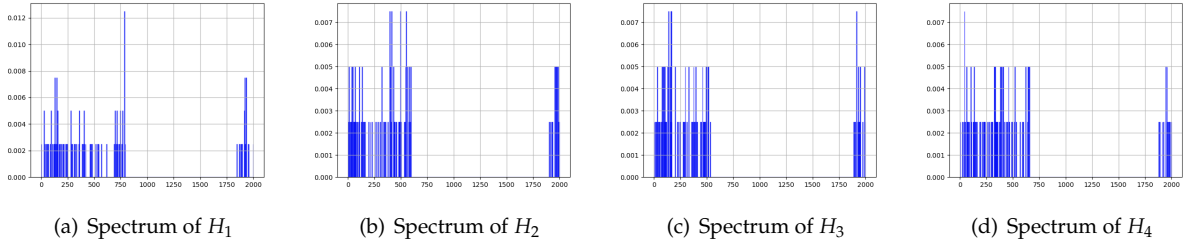


Figure 7: Histogram of eigenvalues of each block in **Case 2** (the homogeneous case). The eigenvalues in the four blocks are sampled from the spectrum of 1st to 4th convolution layers in ResNet18, respectively. All the eigenvalues are shifted and proportionally scaled such that: the objective function is strong convex; the condition number of Hessian equals 2000; their relative ranges are preserved; and the block homogeneity is preserved.

coordinate-wise learning rates according to the initial gradient, but these learning rates are fixed along iteration. The update rule is as follows.

$$w^{t+1} = w^t - \eta(D_{Adam}^0)^{-1} \nabla \mathcal{L}(w) = w^t - \eta(D_{Adam}^0)^{-1} (Hw^t - h), \quad (2)$$

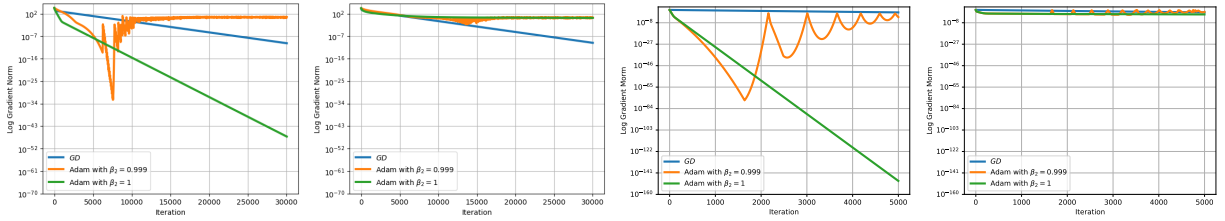
where $D_{Adam}^0 = \text{diag}(\nabla \mathcal{L}(w^0) \circ \nabla \mathcal{L}(w^0))^{\frac{1}{2}}$ and $\nabla \mathcal{L}(w^0) = Hw^0 - h$. When $\beta_2 < 1$, the coordinate-wise learning rates adaptively change along iteration. The update rule is as follows.

$$w^{t+1} = w^t - \eta(D_{Adam}^t)^{-1} \nabla \mathcal{L}(w) = w^t - \eta(D_{Adam}^t)^{-1} (Hw^t - h), \quad (3)$$

where $D_{Adam}^t = \text{diag} \left((1 - \beta_2) \left(\sum_{k=1}^t \beta_2^{t-k} \nabla \mathcal{L}(w^k) \circ \nabla \mathcal{L}(w^k) \right) + \beta^t \text{diag}(\nabla \mathcal{L}(w^0) \circ \nabla \mathcal{L}(w^0)) \right)^{\frac{1}{2}}$ and $\nabla \mathcal{L}(w^k) = Hw^k - h$. We grid search η and use a standard Gaussian random vector as initialization.

We remark that when $\beta_2 < 1$, Adam would repeatedly bounce among non-optimal points, causing non-convergence. This will be shown in Proposition 2.

Summary of experimental observations. We now compare the performance of Adam and GD on these four types of Hessians. The results are shown in Figure 8. For Hessian with heterogeneous blocks like **Case 1 and 3**, GD largely lags behind Adam. For Hessian with homogeneous blocks (**Case 2 and 4**), GD is on par or even better than Adam. We emphasize that all Hessians have the same condition number in these four cases. Further, Hessian of **Case 3 and 4** share all the eigenvalues (not just the extreme ones). The



(a) Hessians with GPT2 blockwise spectrum (b) Hessians with ResNet18 blockwise spectrum (c) Hessians with simplified heterogeneous blocks (d) Hessians with simplified homogeneous blocks

Figure 8: The performance of Adam and GD on quadratic problems. For the construction of Hessian: (a) and (b) use the blockwise spectrum of GPT2 and ResNet18, respectively; (c) and (d) use the implied spectrum described in **Case 3 and 4** in Section 3. The condition numbers of Hessian equal to 2000 for all four cases. For Adam, we use $\beta_1 = 0$ to erase the effect of momentum. We find that: when blocks are heterogeneous, GD largely lags behind Adam; when blocks are homogeneous, GD performs similarly to Adam.

performance gap between Adam and GD is due to the different blockwise spectra caused by the different locations of eigenvalues. We hypothesize that GD performs badly because it uses one single learning rate for all blocks, which cannot handle the heterogeneity among blocks. Such heterogeneity can be better handled using different learning rates across blocks, as designed in Adam.

3.3 Initial Theoretical Results

We now provide initial theoretical results to characterize how GD lags behind Adam in problems with heterogeneous Hessian. Note that classical optimization theory depicts the rate of first-order methods by the condition number of the full Hessian κ . However, we point out that κ is not informative enough to describe the performance gap in Figure 8 since κ is the same in all four cases. To distinguish Adam and GD, we need to utilize more fine-grained quantities like blockwise spectra of sub-matrices.

Unfortunately, the blockwise spectrum is rarely discussed in the optimization area. A most related notion is “block Lipschitz constant” [Beck and Tetrushvili, 2013] for studying block coordinate descent (BCD) type methods, but it was not linked to the performance of SGD or Adam before. To our knowledge, we are not aware of any theory of Adam or GD built on the block diagonal structures or the blockwise spectra of Hessian. Further, there seems to be no result distinguishing the complexity of single-learning-rate methods and the coordinate-wise counterpart, either. We now make an initial attempt in this direction. We first present the lower bound for GD.

Proposition 1. (Lower bound for GD.) Consider $\min_w \mathcal{L}(w) = \frac{1}{2}w^T H w - h^T w$ where $H \in \mathbb{R}^{d \times d}$ is positive definite and $h \in \mathbb{R}^d$. Let w_{GD}^t be the output of GD after t steps. There exists a block diagonal matrix H , h and an initial point w^0 , s.t., for any η , we have:

$$\mathcal{L}(w_{GD}^{t+1}) - \mathcal{L}^* \geq \left(1 - \frac{2}{\kappa + 1}\right) (\mathcal{L}(w_{GD}^t) - \mathcal{L}^*) \quad (4)$$

where κ is the condition number of H .

Proposition 1 shows that GD has complexity $\tilde{O}(\kappa)$ and such complexity is tight. Now we prove that: if we are allowed to choose a customized learning rate for each block sub-matrix H_l , then the complexity will be improved. We call this method blockwise GD (BGD). Note that BGD is impractical to implement since it is hard to choose L learning rates in advance. BGD serves as an artificial method for theoretical understanding.

Blockwise GD (BGD). Choose learning rates $\{\eta_l\}_{l=1}^L$ for all blocks in advance and performs the following:

$$w^{t+1} = w^t - (D_{BGD})^{-1} \nabla \mathcal{L}(w) = w^t - (D_{BGD})^{-1} (H w^t - h),$$

$$\text{where } D_{BGD} = \text{diag} \left(\left(\underbrace{\eta_1, \dots, \eta_1}_{d_1 \text{ times}}, \dots, \underbrace{\eta_L, \dots, \eta_L}_{d_L \text{ times}} \right)^T \right) \in \mathbb{R}^{d \times d}.$$

BGD can be also viewed as a diagonally preconditioned version of GD. We now show that this diagonal preconditioner can significantly improve the complexity of GD.

Theorem 1. (*Upper bound for GD with blockwise learning rate.*) Consider $\min_w \mathcal{L}(w) = \frac{1}{2}w^T H w - h^T w$ where $H \in \mathbb{R}^{d \times d}$ is positive definite and $h \in \mathbb{R}^d$. We assume H is a block diagonal matrix, i.e., $H = \text{diag}(H_1, \dots, H_L)$, where $H_l \in \mathbb{R}^{d_l \times d_l}$ and $d = \sum_{l=1}^L d_l$. Let w_{BGD}^t be the output of BGD after t steps. There exists a set of $\{\eta_l\}_{l=1}^L$ such that:

$$\mathcal{L}(w_{BGD}^{t+1}) - \mathcal{L}^* \leq \max_{l \in [L]} \left(1 - \frac{1}{\kappa_l} \right) (\mathcal{L}(w_{BGD}^t) - \mathcal{L}^*) \quad (5)$$

where κ_l is the condition number of H_l .

Theorem 1 shows that: if we are allowed to choose a learning rate for each H_l , the complexity could be $\tilde{O}(\max_{l \in [L]} \kappa_l)$, in lieu of $\tilde{O}(\kappa)$ as in GD. That is to say, the rate of BGD only depends on the "slowest block". Note that in certain heterogeneous block Hessian such **Case 1** and **3**, κ_l is about $20 \times$ and $2000 \times$ smaller than κ , respectively. In these cases, blockwise-learning-rate methods can be about $20 \times$ and $2000 \times$ faster than single-learning-rate methods like GD, respectively.

Despite the advantages of BGD, it is impractical to find the proper learning rates for all blocks, especially when the number of blocks L is large. Fortunately, these learning rates could be approximated by the preconditioner in Adam, e.g., D_{Adam}^0 in (2). We now provide a complexity bound of Adam.

Assumption 1. (*Bounded initialization.*) The initialization is bounded and is far from the optimal solution:

$$C_{l,1} \lambda_{l,1} \leq \left| [\nabla \mathcal{L}(w^0)]_{l,i} \right| \leq C_{l,2} \lambda_{l,1}, \text{ for } i \in [d_l], l \in [L].$$

Theorem 2. (*Upper bound for Adam with $\beta_2 = 1$.*) Consider the same setting as in Theorem 1 and consider Adam with $\beta_1 = 0$ and $\beta_2 = 1$ as in (2). Assume the initialization satisfies Assumption 1. Let w_{Adam}^t be the output of Adam after t steps. Let $\eta = \min_{l \in [L]} \frac{1}{C_{l,1}}$. We have

$$\mathcal{L}(w_{Adam}^{t+1}) - \mathcal{L}^* \leq \max_{l \in [L]} \left(1 - \frac{1}{\kappa_{Adam,l}} \right) (\mathcal{L}(w_{Adam}^t) - \mathcal{L}^*) \quad (6)$$

where $\kappa_{Adam,l} = r \kappa_l$, $r := \max_{l \in [L]} \left(\frac{C_{l,2}}{C_{l,1}} \right)^2$ and κ_l is the condition number of H_l .

The proofs of all the above theorems are shown in Appendix E. Theorem 2 states that Adam (with $\beta_2 = 1$) has complexity $\tilde{O}(r \cdot \max_{l \in [L]} \kappa_l)$. We remark that condition $\beta_2 = 1$ is necessary because any $\beta_2 < 1$ causes non-convergence issue [Da Silva and Gazeau, 2020, Bock and Weiß, 2019]. We restate their results in Proposition 2. The non-convergence is also observed in Figure 8 (c), where we find that the iterates of Adam quickly converge to near-optimal solutions, and then bounce back. As such, $\beta_2 = 1$ is necessary for asymptotic analysis. As shown in [Da Silva and Gazeau, 2020], the non-convergence is due to the constant learning rate.

Proposition 2. (*Non-convergence of constant-learning-rate Adam with $\beta_2 < 1$.*) [Da Silva and Gazeau, 2020, Proposition 12] Consider $\min_{w \in \mathbb{R}} \mathcal{L}(w) = \frac{1}{2}w^2$. Consider Adam with $\beta_1 = 0$ and $\beta_2 < 1$ as in (3). Let w_{Adam}^t be the output of Adam after t steps. There exists a discrete limit cycle for (3), i.e., Adam produces oscillations and $\liminf_{t \rightarrow \infty} (\mathcal{L}(w_{Adam}^t) - \mathcal{L}^*) > 0$.

We now compare the complexity of Adam and that of GD. By Theorem 2, Adam is faster than GD when $r \cdot \max_{l \in [L]} \kappa_l \leq \kappa$. In the quadratic model with heterogeneous blocks (**Case 3**), our simulation over 1000 trials shows that $r \leq 100$ with probability $\geq \frac{2}{3}$ when using standard Gaussian random initialization. Since

$\max_{l \in [L]} \kappa_l \approx 1$, we have $r \cdot \max_{l \in [L]} \kappa_l \leq 100$, w.h.p., and is $20\times$ smaller than $\kappa = 2000$. So Adam could be $20\times$ faster than GD, w.h.p.. This is indeed observed in Figure 8 where Adam outperforms GD by a significant margin. We summarize the complexity of GD, BGD, and Adam in Table 2.

Optimizer	GD	BGD	Adam with $\beta_1 = 0$ and $\beta_2 = 1$ (2)	Adam with $\beta_1 = 0$ and $\beta_2 < 1$ (3)
Complexity	$\tilde{O}(\kappa)$	$\tilde{O}(\max_{l \in [L]} \kappa_l)$	$\tilde{O}\left(r \cdot \max_{l \in [L]} \kappa_l\right)$	X

Table 2: The complexity of GD, BGD and Adam for minimizing a strongly convex quadratic function with block diagonal Hessian. The symbol **X** means non-convergence. κ and κ_l denote the condition number of the full Hessian and the block submatrix, respectively. $r := \max_{l \in [L]} \left(\frac{C_{l,2}}{C_{l,1}}\right)^2$ and $C_{l,1}, C_{l,2}$ are constants in Assumption 1.

How to obtain a tighter complexity bound of Adam? It is valid to ask whether the complexity upper bound $\kappa_{Adam,l} = r\kappa_l$ can be tightened, e.g., remove the factor of r . We point out it would be difficult if there is no extra structure on H_l . A key technical step is to bound the condition number of the preconditioned matrix $\kappa\left((D_{Adam,l}^0)^{-1}H_l\right)$. Intuitively, a diagonal preconditioner of H_l is expected to be powerful when H_l itself has a near-diagonal structure, e.g., pure diagonal, tridiagonal or diagonal dominant. Unfortunately, it is unclear whether these structures hold in real Transformers. Without any assumption on H_l , we find that the diagonal preconditioner of D_{Adam}^0 could *increase* the condition number. For instance, when using standard Gaussian initialization, in **case 3**, we find $\kappa\left((D_{Adam,l}^0)^{-1}H_l\right)$ equals $3.9\kappa_1, 14.1\kappa_2, 4.2\kappa_3$ for the 3 blocks, respectively (all averaged over 1000 trials). It would be interesting to explore if there are special structures of H_l in real Transformers such that Adam preconditioner can reduce κ_l , rather than increase it. We leave it as a future direction.

Although Adam preconditioner might not always reduce the “local” condition number κ_l , the coefficient in the complexity is now independent of the “global” condition number κ . As argued above, such changes in coefficient could lead to considerable improvement over GD. Such improvement in complexity is attributed to the block diagonal structure in Hessian as well as its heterogeneous blockwise spectrum. To our knowledge, such improvement is not shown in the existing literature. In summary, our theory indicates that: for problems with block heterogeneity, the single-learning rate methods like GD can largely lag behind coordinate-wise learning rate methods like Adam.

4 Related Works

On The failure of SGD on Transformers There is extensive literature studying the difficulties of Transformer training. We summarize these works in Appendix A. We here focus on the literature that explores why SGD fails on Transformers. One representative hypothesis is that SGD fails because it cannot handle the heavy-tailed stochastic noise in language tasks [Zhang et al., 2020]. However, Chen et al. [2021], Kunstner et al. [2023] reported that the gap between Adam and SGD maintains even in the full-batch case with no stochasticity, so there might be other reasons. Further, SGD performs poorly on Vision Transformers on ImageNet (Figure 11), so the data modality (e.g., language or image tasks) might not be as crucial as the architecture. Zhang et al. [2019c] showed that Transformers have the “unbounded smoothness” issue and SGD with gradient clipping performs better than SGD in this case. Although clipping is an effective trick, it does not save SGD from failure as we still observe a huge gap between clipped SGD and Adam³. So there might be other reasons that hamper SGD. Different from these works, we find SGD fails because it uses one single learning rate for all blocks, which cannot handle the Hessian heterogeneity among blocks.

³For all NLP tasks, clipping is performed after backpropagation. So in Figure 11, SGD in NLP tasks essentially refers to clipped SGD.

Understanding of Adam. There was once a long-standing debate on the possible divergence of Adam [Reddi et al., 2018]. The convergence for the unmodified versions is later established in [Shi et al., 2020, Zhang et al., 2022b] for RMSprop and Adam. More convergence analyses of general adaptive gradient methods are listed in Appendix A. We here focus on the literature that explores the benefit of Adam. Xie et al. [2022] show that Adam can help avoid saddle points, which is an orthogonal direction to this work. Wang et al. [2022a], Crawshaw et al. [2022], Li et al. [2023] show that Adam and its variant outperform SGD under relaxed smoothness conditions, based on the intuition that Adam can adaptively change its learning rate along iteration (over time). We pointed out that the theory is not complete: even for quadratic functions where the smoothness is fixed, SGD sometimes fails while Adam works well (Figure 8). This indicates that the benefit of Adam is not merely due to its ability to adaptively change the learning rate over time, and there are other reasons for Adam’s success. We show that an important benefit of Adam is its ability to handle the heterogeneity across blocks (over space).

Bernstein et al. [2018], Wu et al. [2020], Kunstner et al. [2023], Liu et al. [2023] build a relation between Adam and the sign-based methods. Wu et al. [2020] further showed that sign-based methods can be effective when the Hessian is diagonal and satisfies several other properties. However, as put by the authors, it seems “unclear to what extent these properties hold for real problems”. Pan and Li [2023] numerically found that the Adam can reduce the directional sharpness along trajectories, while its relation to fast convergence remains mysterious. A recent work [Jiang et al., 2023] point out that Adam biases the trajectories towards regions where Hessian has “uniform diagonal entries” while SGD cannot. The distribution of Hessian diagonal entries is also investigated in [Liu et al., 2023]. The theory in [Jiang et al., 2023] implies that Adam is faster when the Hessian is diagonal. However, as argued above, it is unclear whether the diagonal Hessian commonly holds in real problems. In fact, we find the Hessian is closer to a block-diagonal (instead of pure diagonal) structure on some small Transformers. In these cases, blockwise eigenvalues carry more information than diagonal entries, providing extra details such as the location of eigenvalues. We find that these extra details are important for distinguishing Adam and SGD.

Hessian Spectrum Analysis. There are several important attempts to explore the Hessian spectrum of MLPs and CNNs. Sagun et al. [2016, 2017], Chaudhari et al. [2019] found that the Hessian spectra of MLPs and CNNs consist of a “bulk” together with a few “outliers”. Pappayan [2020], Wu et al. [2020], Liao and Mahoney [2021] further characterized the bulks and outliers in theory. Pappayan [2018, 2019] numerically built the relation between these “outliers” and the Gauss-Newton matrix. Sankar et al. [2021] numerically explored the relation between Hessian of CNNs and Gauss-Newton matrix in each layer. They further showed that most CNN layers contribute similarly to the overall loss surface. We find that this result is restricted to CNNs and does not hold on Transformers due to the heterogeneity. Gur-Ari et al. [2018] showed that for MLPs and CNNs, gradient descent converges to a small subspace spanned by a few top eigenvectors of the Hessian. Yao et al. [2018], Zhang et al. [2019b] explored the relation between the Hessian spectrum of CNNs and some training phenomena such as the effect of batch sizes. Ghorbani et al. [2019], Yao et al. [2020] focused on explaining the effectiveness of techniques such as BatchNorm. Note that all these works are restricted to MLPs and CNNs, while we study the Hessian of Transformers (in addition to CNNs and MLPs) as well as its impacts on different optimizers.

5 Conclusion

In this work, we investigate the failure mode of SGD on Transformers through the lens of Hessian. By numerically explore various Transformers, CNNs, MLPs and quadratic problems, we establish a phenomenon called block heterogeneity in Hessian and link it to the failure of SGD. We point out that SGD fails because it applies one single learning rate for all blocks, which cannot handle the heterogeneity among blocks. Initial theory are provided to support the claim.

References

- J. Achiam, S. Adler, S. Agarwal, L. Ahmad, I. Akkaya, F. L. Aleman, D. Almeida, J. Altenschmidt, S. Altman, S. Anadkat, et al. Gpt-4 technical report. *arXiv preprint arXiv:2303.08774*, 2023.
- R. P. Adams, J. Pennington, M. J. Johnson, J. Smith, Y. Ovadia, B. Patton, and J. Saunderson. Estimating the spectral density of large implicit matrices. *arXiv preprint arXiv:1802.03451*, 2018.
- H. Avron and S. Toledo. Randomized algorithms for estimating the trace of an implicit symmetric positive semi-definite matrix. *Journal of the ACM (JACM)*, 58(2):1–34, 2011.
- T. Bachlechner, B. P. Majumder, H. Mao, G. Cottrell, and J. McAuley. Rezero is all you need: Fast convergence at large depth. In *Uncertainty in Artificial Intelligence*, pages 1352–1361. PMLR, 2021.
- Z. Bai and G. H. Golub. Bounds for the trace of the inverse and the determinant of symmetric positive definite matrices. *Annals of Numerical Mathematics*, 4:29–38, 1996.
- Z. Bai, G. Fahey, and G. Golub. Some large-scale matrix computation problems. *Journal of Computational and Applied Mathematics*, 74(1-2):71–89, 1996.
- A. Beck and L. Tetruashvili. On the convergence of block coordinate descent type methods. *SIAM journal on Optimization*, 23(4):2037–2060, 2013.
- J. Bernstein, Y.-X. Wang, K. Azizzadenesheli, and A. Anandkumar. signsgd: Compressed optimisation for non-convex problems. In *International Conference on Machine Learning*, pages 560–569. PMLR, 2018.
- S. Bock and M. Weiß. Non-convergence and limit cycles in the adam optimizer. In *Artificial Neural Networks and Machine Learning—ICANN 2019: Deep Learning: 28th International Conference on Artificial Neural Networks, Munich, Germany, September 17–19, 2019, Proceedings, Part II 28*, pages 232–243. Springer, 2019.
- C. Brezinski. A direct proof of the christoffel-darboux identity and its equivalence to the recurrence relationship. *Journal of Computational and Applied Mathematics*, 32(1-2):17–25, 1990.
- P. Chaudhari, A. Choromanska, S. Soatto, Y. LeCun, C. Baldassi, C. Borgs, J. Chayes, L. Sagun, and R. Zecchina. Entropy-sgd: Biasing gradient descent into wide valleys. *Journal of Statistical Mechanics: Theory and Experiment*, 2019(12):124018, 2019.
- C. Chen, L. Shen, F. Zou, and W. Liu. Towards practical adam: Non-convexity, convergence theory, and mini-batch acceleration. *The Journal of Machine Learning Research*, 23(1):10411–10457, 2022.
- J. Chen, F. Kunstner, and M. Schmidt. Heavy-tailed noise does not explain the gap between sgd and adam on transformers. In *13th Annual Workshop on Optimization for Machine Learning*, 2021.
- M. X. Chen, O. Firat, A. Bapna, M. Johnson, W. Macherey, G. Foster, L. Jones, N. Parmar, M. Schuster, Z. Chen, et al. The best of both worlds: Combining recent advances in neural machine translation. *arXiv preprint arXiv:1804.09849*, 2018.
- X. Chen, S. Liu, R. Sun, and M. Hong. On the convergence of a class of adam-type algorithms for non-convex optimization. In *7th International Conference on Learning Representations, ICLR 2019*, 2019.
- A. Chowdhery, S. Narang, J. Devlin, M. Bosma, G. Mishra, A. Roberts, P. Barham, H. W. Chung, C. Sutton, S. Gehrmann, et al. Palm: Scaling language modeling with pathways. *Journal of Machine Learning Research*, 24(240):1–113, 2023.
- R. Collobert. Large scale machine learning. Technical report, Université de Paris VI, 2004.
- M. Crawshaw, M. Liu, F. Orabona, W. Zhang, and Z. Zhuang. Robustness to unbounded smoothness of generalized signsgd. *Advances in Neural Information Processing Systems*, 35:9955–9968, 2022.

- J. K. Cullum and R. A. Willoughby. *Lanczos algorithms for large symmetric eigenvalue computations: Vol. I: Theory*. SIAM, 2002.
- A. B. Da Silva and M. Gazeau. A general system of differential equations to model first-order adaptive algorithms. *The Journal of Machine Learning Research*, 21(1):5072–5113, 2020.
- T. Dao, D. Fu, S. Ermon, A. Rudra, and C. Ré. Flashattention: Fast and memory-efficient exact attention with io-awareness. *Advances in Neural Information Processing Systems*, 35:16344–16359, 2022.
- A. Défossez, L. Bottou, F. Bach, and N. Usunier. A simple convergence proof of adam and adagrad. *Transactions on Machine Learning Research*, 2022.
- M. Dehghani, J. Djolonga, B. Mustafa, P. Padlewski, J. Heek, J. Gilmer, A. P. Steiner, M. Caron, R. Geirhos, I. Alabdulmohsin, et al. Scaling vision transformers to 22 billion parameters. In *International Conference on Machine Learning*, pages 7480–7512. PMLR, 2023.
- J. Devlin, M.-W. Chang, K. Lee, and K. Toutanova. Bert: Pre-training of deep bidirectional transformers for language understanding. *arXiv preprint arXiv:1810.04805*, 2018.
- Y. Dong, J.-B. Cordonnier, and A. Loukas. Attention is not all you need: Pure attention loses rank doubly exponentially with depth. In *International Conference on Machine Learning*, pages 2793–2803. PMLR, 2021.
- A. Dosovitskiy, L. Beyer, A. Kolesnikov, D. Weissenborn, X. Zhai, T. Unterthiner, M. Dehghani, M. Minderer, G. Heigold, S. Gelly, et al. An image is worth 16x16 words: Transformers for image recognition at scale. *arXiv preprint arXiv:2010.11929*, 2020.
- J. Duchi, E. Hazan, and Y. Singer. Adaptive subgradient methods for online learning and stochastic optimization. *Journal of machine learning research*, 12(7), 2011.
- J. F. Epperson. An introduction to numerical methods and analysis. 2013.
- S. Gadat and I. Gavra. Asymptotic study of stochastic adaptive algorithms in non-convex landscape. *The Journal of Machine Learning Research*, 23(1):10357–10410, 2022.
- B. Ghorbani, S. Krishnan, and Y. Xiao. An investigation into neural net optimization via hessian eigenvalue density. In *International Conference on Machine Learning*, pages 2232–2241. PMLR, 2019.
- G. Goh. Why momentum really works. *Distill*, 2017. doi: 10.23915/distill.00006. URL <http://distill.pub/2017/momentum>.
- G. H. Golub and G. Meurant. *Matrices, moments and quadrature with applications*, volume 30. Princeton University Press, 2009.
- G. H. Golub and Z. Strakoš. Estimates in quadratic formulas. *Numerical Algorithms*, 8:241–268, 1994.
- G. H. Golub and J. H. Welsch. Calculation of gauss quadrature rules. *Mathematics of computation*, 23(106): 221–230, 1969.
- B. Goujaud, D. Scieur, A. Dieuleveut, A. B. Taylor, and F. Pedregosa. Super-acceleration with cyclical step-sizes. In *International Conference on Artificial Intelligence and Statistics*, pages 3028–3065. PMLR, 2022.
- A. Gu and T. Dao. Mamba: Linear-time sequence modeling with selective state spaces. *arXiv preprint arXiv:2312.00752*, 2023.
- G. Gur-Ari, D. A. Roberts, and E. Dyer. Gradient descent happens in a tiny subspace. *arXiv preprint arXiv:1812.04754*, 2018.
- K. He, X. Zhang, S. Ren, and J. Sun. Deep residual learning for image recognition. In *Proceedings of the IEEE conference on computer vision and pattern recognition*, pages 770–778, 2016.

- X. S. Huang, F. Perez, J. Ba, and M. Volkovs. Improving transformer optimization through better initialization. In *International Conference on Machine Learning*, pages 4475–4483. PMLR, 2020.
- M. F. Hutchinson. A stochastic estimator of the trace of the influence matrix for laplacian smoothing splines. *Communications in Statistics-Simulation and Computation*, 18(3):1059–1076, 1989.
- K. Jiang, D. Malik, and Y. Li. How does adaptive optimization impact local neural network geometry? *Advances in Neural Information Processing Systems*, 36, 2023.
- J. Kaplan, S. McCandlish, T. Henighan, T. B. Brown, B. Chess, R. Child, S. Gray, A. Radford, J. Wu, and D. Amodei. Scaling laws for neural language models. *arXiv preprint arXiv:2001.08361*, 2020.
- D. P. Kingma and J. Ba. Adam: A method for stochastic optimization. *arXiv preprint arXiv:1412.6980*, 2014.
- F. Kunstner, J. Chen, J. W. Lavington, and M. Schmidt. Noise is not the main factor behind the gap between sgd and adam on transformers, but sign descent might be. *arXiv preprint arXiv:2304.13960*, 2023.
- C. Lanczos. An iteration method for the solution of the eigenvalue problem of linear differential and integral operators. 1950.
- Y. LeCun, L. Bottou, Y. Bengio, and P. Haffner. Gradient-based learning applied to document recognition. *Proceedings of the IEEE*, 86(11):2278–2324, 1998.
- Y. LeCun, L. Bottou, G. B. Orr, and K.-R. Müller. Efficient backprop. In *Neural networks: Tricks of the trade*, pages 9–50. Springer, 2002.
- H. Li, A. Rakhlin, and A. Jadbabaie. Convergence of adam under relaxed assumptions. *Advances in Neural Information Processing Systems*, 36, 2023.
- Z. Liao and M. W. Mahoney. Hessian eigenspectra of more realistic nonlinear models. *Advances in Neural Information Processing Systems*, 34:20104–20117, 2021.
- L. Lin, Y. Saad, and C. Yang. Approximating spectral densities of large matrices. *SIAM review*, 58(1):34–65, 2016.
- H. Liu, Z. Li, D. Hall, P. Liang, and T. Ma. Sophia: A scalable stochastic second-order optimizer for language model pre-training. *arXiv preprint arXiv:2305.14342*, 2023.
- L. Liu, H. Jiang, P. He, W. Chen, X. Liu, J. Gao, and J. Han. On the variance of the adaptive learning rate and beyond. arxiv 2019. *arXiv preprint arXiv:1908.03265*, 2019.
- L. Liu, X. Liu, J. Gao, W. Chen, and J. Han. Understanding the difficulty of training transformers. *arXiv preprint arXiv:2004.08249*, 2020.
- I. Loshchilov and F. Hutter. Decoupled weight decay regularization. *arXiv preprint arXiv:1711.05101*, 2017.
- L. Luo, Y. Xiong, Y. Liu, and X. Sun. Adaptive gradient methods with dynamic bound of learning rate. In *International Conference on Learning Representations*, 2018.
- J. Martens and R. Grosse. Optimizing neural networks with kronecker-factored approximate curvature. In *International conference on machine learning*, pages 2408–2417. PMLR, 2015.
- W. Merrill, V. Ramanujan, Y. Goldberg, R. Schwartz, and N. Smith. Effects of parameter norm growth during transformer training: Inductive bias from gradient descent. *arXiv preprint arXiv:2010.09697*, 2020.
- I. Molybog, P. Albert, M. Chen, Z. DeVito, D. Esiobu, N. Goyal, P. S. Koura, S. Narang, A. Poulton, R. Silva, et al. A theory on adam instability in large-scale machine learning. *arXiv preprint arXiv:2304.09871*, 2023.

- Y. Nesterov. *Introductory lectures on convex optimization: A basic course*, volume 87. Springer Science & Business Media, 2013.
- T. Q. Nguyen and J. Salazar. Transformers without tears: Improving the normalization of self-attention. *arXiv preprint arXiv:1910.05895*, 2019.
- L. Noci, S. Anagnostidis, L. Biggio, A. Orvieto, S. P. Singh, and A. Lucchi. Signal propagation in transformers: Theoretical perspectives and the role of rank collapse. *Advances in Neural Information Processing Systems*, 35: 27198–27211, 2022.
- Y. Pan and Y. Li. Toward understanding why adam converges faster than sgd for transformers. *arXiv preprint arXiv:2306.00204*, 2023.
- V. Pappas. The full spectrum of deepnet Hessians at scale: Dynamics with sgd training and sample size. *arXiv preprint arXiv:1811.07062*, 2018.
- V. Pappas. Measurements of three-level hierarchical structure in the outliers in the spectrum of deepnet Hessians. *arXiv preprint arXiv:1901.08244*, 2019.
- V. Pappas. Traces of class/cross-class structure pervade deep learning spectra. *The Journal of Machine Learning Research*, 21(1):10197–10260, 2020.
- B. A. Pearlmutter. Fast exact multiplication by the Hessian. *Neural computation*, 6(1):147–160, 1994.
- A. Radford, J. Wu, R. Child, D. Luan, D. Amodei, I. Sutskever, et al. Language models are unsupervised multitask learners. *OpenAI blog*, 1(8):9, 2019.
- J. Rasley, S. Rajbhandari, O. Ruwase, and Y. He. Deepspeed: System optimizations enable training deep learning models with over 100 billion parameters. In *Proceedings of the 26th ACM SIGKDD International Conference on Knowledge Discovery & Data Mining*, pages 3505–3506, 2020.
- S. J. Reddi, S. Kale, and S. Kumar. On the convergence of adam and beyond. In *International Conference on Learning Representations*, 2018.
- N. Roux, P.-A. Manzagol, and Y. Bengio. Topmoumoute online natural gradient algorithm. *Advances in neural information processing systems*, 20, 2007.
- Y. Saad. *Numerical methods for large eigenvalue problems: revised edition*. SIAM, 2011.
- L. Sagun, L. Bottou, and Y. LeCun. Eigenvalues of the Hessian in deep learning: Singularity and beyond. *arXiv preprint arXiv:1611.07476*, 2016.
- L. Sagun, U. Evci, V. U. Guney, Y. Dauphin, and L. Bottou. Empirical analysis of the Hessian of over-parametrized neural networks. *arXiv preprint arXiv:1706.04454*, 2017.
- A. R. Sankar, Y. Khasbage, R. Vigneswaran, and V. N. Balasubramanian. A deeper look at the Hessian eigenspectrum of deep neural networks and its applications to regularization. In *Proceedings of the AAAI Conference on Artificial Intelligence*, volume 35, pages 9481–9488, 2021.
- N. Shi, D. Li, M. Hong, and R. Sun. Rmsprop converges with proper hyper-parameter. In *International Conference on Learning Representations*, 2020.
- K. Simonyan and A. Zisserman. Very deep convolutional networks for large-scale image recognition. *arXiv preprint arXiv:1409.1556*, 2014.
- R. Sun. Optimization for deep learning: theory and algorithms. *arXiv preprint arXiv:1912.08957*, 2019.
- R. Sun and Y. Ye. Worst-case complexity of cyclic coordinate descent: $O(n^2)$ gap with randomized version. *Mathematical Programming*, 185:487–520, 2021.

- S. Ubaru, J. Chen, and Y. Saad. Fast estimation of $\text{tr}(f(a))$ via stochastic lanczos quadrature. *SIAM Journal on Matrix Analysis and Applications*, 38(4):1075–1099, 2017.
- A. Vaswani, N. Shazeer, N. Parmar, J. Uszkoreit, L. Jones, A. N. Gomez, L. Kaiser, and I. Polosukhin. Attention is all you need. *Advances in neural information processing systems*, 30, 2017.
- B. Wang, Y. Zhang, H. Zhang, Q. Meng, Z.-M. Ma, T.-Y. Liu, and W. Chen. Provable adaptivity in adam. *arXiv preprint arXiv:2208.09900*, 2022a.
- B. Wang, J. Fu, H. Zhang, N. Zheng, and W. Chen. Closing the gap between the upper bound and lower bound of adam’s iteration complexity. *Advances in Neural Information Processing Systems*, 36, 2023a.
- B. Wang, H. Zhang, Z. Ma, and W. Chen. Convergence of adagrad for non-convex objectives: Simple proofs and relaxed assumptions. In *The Thirty Sixth Annual Conference on Learning Theory*, pages 161–190. PMLR, 2023b.
- H. Wang, S. Ma, L. Dong, S. Huang, D. Zhang, and F. Wei. Deepnet: Scaling transformers to 1,000 layers. *arXiv preprint arXiv:2203.00555*, 2022b.
- Q. Wang, B. Li, T. Xiao, J. Zhu, C. Li, D. F. Wong, and L. S. Chao. Learning deep transformer models for machine translation. *arXiv preprint arXiv:1906.01787*, 2019.
- Wikipedia. Gaussian quadrature — Wikipedia, the free encyclopedia, 2023. URL https://en.wikipedia.org/w/index.php?title=Gaussian_quadrature&oldid=1191539517. [Online; accessed 20-January-2024].
- M. Wortsman, P. J. Liu, L. Xiao, K. Everett, A. Alemi, B. Adlam, J. D. Co-Reyes, I. Gur, A. Kumar, R. Novak, et al. Small-scale proxies for large-scale transformer training instabilities. *arXiv preprint arXiv:2309.14322*, 2023.
- Y. Wu, X. Zhu, C. Wu, A. Wang, and R. Ge. Dissecting hessian: Understanding common structure of hessian in neural networks. *arXiv preprint arXiv:2010.04261*, 2020.
- Z. Xie, X. Wang, H. Zhang, I. Sato, and M. Sugiyama. Adaptive inertia: Disentangling the effects of adaptive learning rate and momentum. In *International conference on machine learning*, pages 24430–24459. PMLR, 2022.
- R. Xiong, Y. Yang, D. He, K. Zheng, S. Zheng, C. Xing, H. Zhang, Y. Lan, L. Wang, and T. Liu. On layer normalization in the transformer architecture. In *International Conference on Machine Learning*, pages 10524–10533. PMLR, 2020.
- A. Yang, B. Xiao, B. Wang, B. Zhang, C. Bian, C. Yin, C. Lv, D. Pan, D. Wang, D. Yan, et al. Baichuan 2: Open large-scale language models. *arXiv preprint arXiv:2309.10305*, 2023.
- G. Yang, E. J. Hu, I. Babuschkin, S. Sidor, X. Liu, D. Farhi, N. Ryder, J. Pachocki, W. Chen, and J. Gao. Tensor programs v: Tuning large neural networks via zero-shot hyperparameter transfer. *arXiv preprint arXiv:2203.03466*, 2022.
- Z. Yao, A. Gholami, Q. Lei, K. Keutzer, and M. W. Mahoney. Hessian-based analysis of large batch training and robustness to adversaries. *Advances in Neural Information Processing Systems*, 31, 2018.
- Z. Yao, A. Gholami, K. Keutzer, and M. W. Mahoney. Pyhessian: Neural networks through the lens of the hessian. In *2020 IEEE international conference on big data (Big data)*, pages 581–590. IEEE, 2020.
- M. Zaheer, S. Reddi, D. Sachan, S. Kale, and S. Kumar. Adaptive methods for nonconvex optimization. *Advances in neural information processing systems*, 31, 2018.

- A. Zeng, X. Liu, Z. Du, Z. Wang, H. Lai, M. Ding, Z. Yang, Y. Xu, W. Zheng, X. Xia, et al. Glm-130b: An open bilingual pre-trained model. *arXiv preprint arXiv:2210.02414*, 2022.
- S. Zhai, T. Likhomanenko, E. Littwin, D. Busbridge, J. Ramapuram, Y. Zhang, J. Gu, and J. M. Susskind. Stabilizing transformer training by preventing attention entropy collapse. In *International Conference on Machine Learning*, pages 40770–40803. PMLR, 2023.
- B. Zhang, I. Titov, and R. Sennrich. Improving deep transformer with depth-scaled initialization and merged attention. *arXiv preprint arXiv:1908.11365*, 2019a.
- G. Zhang, L. Li, Z. Nado, J. Martens, S. Sachdeva, G. Dahl, C. Shallue, and R. B. Grosse. Which algorithmic choices matter at which batch sizes? insights from a noisy quadratic model. *Advances in neural information processing systems*, 32, 2019b.
- J. Zhang, T. He, S. Sra, and A. Jadbabaie. Why gradient clipping accelerates training: A theoretical justification for adaptivity. *arXiv preprint arXiv:1905.11881*, 2019c.
- J. Zhang, S. P. Karimireddy, A. Veit, S. Kim, S. Reddi, S. Kumar, and S. Sra. Why are adaptive methods good for attention models? *Advances in Neural Information Processing Systems*, 33:15383–15393, 2020.
- S. Zhang, S. Roller, N. Goyal, M. Artetxe, M. Chen, S. Chen, C. Dewan, M. Diab, X. Li, X. V. Lin, et al. Opt: Open pre-trained transformer language models. *arXiv preprint arXiv:2205.01068*, 2022a.
- Y. Zhang, C. Chen, N. Shi, R. Sun, and Z.-Q. Luo. Adam can converge without any modification on update rules. *Advances in Neural Information Processing Systems*, 35:28386–28399, 2022b.
- D. Zhou, J. Chen, Y. Cao, Y. Tang, Z. Yang, and Q. Gu. On the convergence of adaptive gradient methods for nonconvex optimization. *arXiv preprint arXiv:1808.05671*, 2018.
- F. Zou, L. Shen, Z. Jie, W. Zhang, and W. Liu. A sufficient condition for convergences of adam and rmsprop. In *Proceedings of the IEEE/CVF Conference on computer vision and pattern recognition*, pages 11127–11135, 2019.

A More Related Works

On the difficulties of Transformer training. Transformers are known to be difficult to train. Researchers have attributed the training difficulties to various phenomena in different components of Transformers, including: the logits divergence or the rank degeneracy in the outputs of attention layers [Dong et al., 2021, Noci et al., 2022, Wortsman et al., 2023, Zhai et al., 2023, Dehghani et al., 2023, Chowdhery et al., 2023]; the growth of parameter norm in attention layers [Merrill et al., 2020]; over-reliance on residue branches [Liu et al., 2020]; and some negative impact of layer norm [Chen et al., 2018, Zhang et al., 2019a, Huang et al., 2020]. These phenomena have a strong correlation with gradient vanishing or explosion in Transformers [Zhang et al., 2019a, Liu et al., 2020, Huang et al., 2020, Xiong et al., 2020, Noci et al., 2022, Wang et al., 2022b, Wortsman et al., 2023, Molybog et al., 2023], which leads to training difficulties.

Several solutions have been proposed. Liu et al. [2020] numerically observed that adaptive gradient methods can (partly) overcome gradient vanishing by giving “consistent update magnitude”, while it seems unclear how consistent update magnitude would help optimization in principle. Researchers further develop training tricks such as warmup learning rate [Liu et al., 2019, Xiong et al., 2020], temperature scaling [Noci et al., 2022], better initialization [Zhang et al., 2019a, Huang et al., 2020, Wang et al., 2022b, Bachlechner et al., 2021, Yang et al., 2022], and variants of Layer Norm [Nguyen and Salazar, 2019, Wang et al., 2019, Xiong et al., 2020, Wang et al., 2022b, Dehghani et al., 2023]. Recent researchers also suggest using z-loss regularization [Chowdhery et al., 2023, Yang et al., 2023] and tuning hyperparameters of Adam [Zhang et al., 2022b, Wortsman et al., 2023]. All these tricks can help mitigate gradient explosion or vanishing. Nevertheless, training large-scale Transformers remains challenging [Zhang et al., 2022a, Zeng et al., 2022, Wortsman et al., 2023, Molybog et al., 2023, Chowdhery et al., 2023]. Different from all aforementioned works, we investigate the training difficulties of Transformers through the eigenvalues of Hessian. We establish a strong correlation between the blockwise Hessian spectra of Transformers and the failure of SGD. We realize that our attempt is just a first step towards understanding Transformer training, and we believe there is rich information hidden in Hessian and we leave more fine-grained analysis as future works.

Convergence analysis of adaptive gradient methods There is extensive convergence analysis for adaptive gradient methods. For instance, researchers study the convergence of AMSGrad [Reddi et al., 2018, Zhou et al., 2018], RMSprop [Zaheer et al., 2018], AdaFom [Chen et al., 2019], AdaBound [Luo et al., 2018], and Adam with iterate-dependent hyperparameters [Zou et al., 2019, Chen et al., 2022, Gadat and Gavra, 2022]. The convergence of Adam is also explored in [Défossez et al., 2022, Wang et al., 2023a]. There is also an active line of theoretical research on the convergence of AdaGrad [Duchi et al., 2011], we recommend [Wang et al., 2023b] for more detailed introduction. In this work, we do not focus on the convergence analysis. Rather, we explore the quantitative difference between the loss landscape of CNNs and Transformers and how it impact the behaviors of SGD and Adam.

B More Preliminaries

B.1 Preliminaries on Optimizers

Here we provide a detailed description of the optimizers mentioned in the full script. We consider the minimizing $\mathcal{L}(w) \equiv \frac{1}{n} \sum_{i=1}^n \mathcal{L}_i(w)$, where n is the number of minibatches, $\mathcal{L}_i(w)$ is the loss of i -th minibatch and $w \in \mathbb{R}^d$ is the neural network parameters. We denote the gradient of the training loss w.r.t. neural network parameters as $\nabla \mathcal{L}(w) \in \mathbb{R}^d$. We use $\nabla \mathcal{L}_i(w) \in \mathbb{R}^d$ to denote the i -th minibatch counterparts. We use w^t to denote the variable at the t -th step. In Algorithm 2 and 3, \circ , division and square-root are elementwise operations. In the line 7 and 8 of Algorithm 2, $(\beta_1)^t$ and $(\beta_2)^t$ indicates the t -th power of β_1, β_2 . In the PyTorch default setting, $(\beta_1, \beta_2, \epsilon) = (0.9, 0.999, 1e-8)$ for Adam and $\beta_1 = 0.9$ for SGD.

Algorithm 1 Stochastic Gradient Descent with Momentum (SGD)

- 1: Initialize w^0 and choose $0 \leq \beta_1 < 1$ and $\eta_0 > 0$
 - 2: **for** $t = 1 \rightarrow \infty$ **do**
 - 3: Uniformly sample τ^t from the index set $\{1, 2, \dots, n\}$
 - 4: $m^t = \beta_1 m^t + \nabla f_{\tau^t}(x^t)$
 - 5: $x^{t+1} = x^t - \eta_t m^t$
 - 6: **end for**
-

Algorithm 2 AdamW

- 1: Initialize $x^0, m^0 = v^0 = 0, 0 \leq \beta_1 < 1, 0 \leq \beta_2 < 1, \epsilon > 0, \eta^0 > 0$, and weight decay coefficient λ
 - 2: **for** $t = 1 \rightarrow \infty$ **do**
 - 3: Uniformly sample τ^t from the index set $\{1, 2, \dots, n\}$
 - 4: $w^{t+1} = w^t - \eta^t \lambda w^t$
 - 5: $m^t = \beta_1 m^t + (1 - \beta_1) \nabla \mathcal{L}_{\tau^t}(w^t)$
 - 6: $v^t = \beta_2 v^t + (1 - \beta_2) \nabla \mathcal{L}_{\tau^t}(w^t) \circ \nabla \mathcal{L}_{\tau^t}(w^t)$
 - 7: $\hat{m}^t = \frac{m^t}{1 - (\beta_1)^t}$
 - 8: $\hat{v}^t = \frac{v^t}{1 - (\beta_2)^t}$
 - 9: $w^{t+1} = w^{t+1} - \eta_t \frac{\hat{m}^t}{\sqrt{\hat{v}^t + \epsilon}}$
 - 10: **end for**
-

Algorithm 3 Adam with no bias correction

- 1: Initialize $x^0, m^0 = \nabla \mathcal{L}_{\tau^t}(w^0), v^0 = \nabla \mathcal{L}_{\tau^t}(w^0) \circ \nabla \mathcal{L}_{\tau^t}(w^0), 0 \leq \beta_1 < 1, 0 \leq \beta_2 < 1, \epsilon > 0, \eta^0 > 0$
 - 2: **for** $t = 1 \rightarrow \infty$ **do**
 - 3: Uniformly sample τ^t from the index set $\{1, 2, \dots, n\}$
 - 4: $m^t = \beta_1 m^t + (1 - \beta_1) \nabla \mathcal{L}_{\tau^t}(w^t)$
 - 5: $v^t = \beta_2 v^t + (1 - \beta_2) \nabla \mathcal{L}_{\tau^t}(w^t) \circ \nabla \mathcal{L}_{\tau^t}(w^t)$
 - 6: $w^{t+1} = w^{t+1} - \eta_t \frac{m^t}{\sqrt{v^t + \epsilon}}$
 - 7: **end for**
-

B.2 Preliminaries on the Stochastic Lanczos Quadrature Method

Additional notations. Given a real symmetric matrix $H \in \mathbb{R}^{d \times d}$, we denote $\text{tr}(H)$ as its trace and $Q^T \Lambda Q$ as its spectral decomposition, where $Q = [q_1, \dots, q_d]$, $\Lambda = \text{diag}(\lambda_1, \dots, \lambda_d)$ and $\lambda_1 \geq \lambda_2 \geq \dots \geq \lambda_d$. We denote the condition number of H as $\kappa = \lambda_1/\lambda_d$. We define matrix function as $f(H) := Q^T f(\Lambda) Q$, where $f(\Lambda) = \text{diag}(f(\lambda_1), \dots, f(\lambda_d)) \in \mathbb{R}^{d \times d}$. We use \mathbb{N} to denote the set of positive integers. We use $\|\cdot\|_2$ to denote the Euclidean norm.

Approximation of the Hessian spectrum can be formulated as a trace estimation problem, as introduced in [Lin et al., 2016, Ubaru et al., 2017]. First, the spectrum (eigenvalue density) of Hessian H can be written as: $\phi(t) = \frac{1}{d} \sum_{i=1}^d \delta(t - \lambda_i)$, where λ_i are the eigenvalues of H and δ is the Dirac δ -function. Then, we replace the delta functions by a Gaussian blurring function: $\phi(t) \approx g(t) := \frac{1}{d} \sum_{i=1}^d f(\lambda_i)$, where $f(\lambda) := \frac{1}{\sigma\sqrt{2\pi}} \exp\left(-\frac{(t-\lambda)^2}{2\sigma^2}\right)$. By definition of matrix function, it is easy to see that $g(t) = \frac{1}{d} \text{tr}(f(H))$. As such, spectrum approximation could be formulated as a trace estimation problem, i.e., estimating $\frac{1}{d} \text{tr}(f(H))$, where $H \in \mathbb{R}^{d \times d}$ is a real symmetric matrix.

Trace estimation problems could be solved efficiently by the Stochastic Lanczos Quadrature Method (SLQ) [Golub and Strakoš, 1994]. For the ease of readers, we provide a detailed description of SLQ in our context. SLQ consists of the following steps.

Step 1. We approximate the trace of matrix function as $\frac{1}{d} \text{tr}(f(H)) = \mathbb{E}(v^T f(H) v) \approx \frac{1}{n_v} \sum_{i=1}^{n_v} v_i^T f(H) v_i$, where $v = u/\|u\|_2$ and u is a Rademacher random vector (each entry of u independently takes ± 1 with probability $1/2$). This step is called Hutchinson's estimation [Hutchinson, 1989].

Note that we can also replace the Rademacher random vector u by a unit Gaussian vector (i.e., $u \sim N(0, I_{d \times d})$) and the unbiasedness still holds [Avron and Toledo, 2011]. In our implementation, we sample $u \sim N(0, I_{d \times d})$ because there is an efficient built-in PyTorch function for generating Gaussian vectors.

SLQ estimates $v_i^T f(H) v_i$ for $i \in [n_v]$ and then takes the average. To understand SLQ, we only need to understand how it estimates each individual quadratic form. To simplify the notation regarding i , from now on, we will discuss how to estimate $v^T f(H) v$, where $v = u/\|u\|_2$ and u is a unit Gaussian vector.

Step 2-1. We rewrite $v^T f(H) v$ as a Riemann-Stieltjes integral [Golub and Meurant, 2009]:

$$v^T f(H) v = \sum_{i=1}^d (v^T q_i)^2 f(\lambda_i) = \int_{\lambda_d}^{\lambda_1} f(\lambda) d\mu(\lambda), \quad (7)$$

where μ is a measure on (\mathbb{R}, \mathbb{B}) defined as follows ($\mu(\lambda)$ denotes the measure of set $\{x; x \leq \lambda\}$):

$$\mu(\lambda) = \begin{cases} 0 & \lambda < \lambda_d \\ \sum_{i=1}^k (v^T q_i)^2 & \lambda_k \leq \lambda < \lambda_{k+1} \\ \sum_{i=1}^d (v^T q_i)^2 & \lambda \geq \lambda_1 \end{cases} \quad (8)$$

Step 2-2. Unfortunately, this integral is difficult to compute. This is because the measure μ are related to the eigen-pairs of H , which are unknown. It seems unclear how to directly integrate over an unknown measure. As such, we further approximate this integral by a computationally friendly quantity, such as:

$$\int_{\lambda_d}^{\lambda_1} f(\lambda) d\mu(\lambda) \approx \sum_{j=1}^m c_j f(x_j). \quad (9)$$

We hope to design $\{(c_j, x_j)\}_{j=1}^m$ with a reasonable number of m such that the estimation error is small. Fortunately, the Gaussian Quadrature method provides a generic design principle of $\{(c_j, x_j)\}_{j=1}^m$ [Golub and Meurant, 2009, Epperson, 2013]. It is proved that: when $f(\lambda)$ is not "too complicated" (e.g. $f(\lambda)$ is

a polynomial), then there exists $\{(c_j, x_j)\}_{j=1}^m$ which gives a high quality estimation of integral (7). The required number of m is related to "how complicated the $f(\lambda)$ is". Such $\{(c_j, x_j)\}_{j=1}^m$ are called the Gaussian Quadrature rules. c_j and x_j are called the "weights" and the "nodes" of the Gaussian Quadrature rules. A representative theorem is as follows: when $f(\lambda)$ is a polynomial with degree $< 2m$, then the Gaussian Quadrature rules give the exact approximation of integral (7).

Theorem 3. [Rewritten based on [Wikipedia, 2023]] Suppose we have a sequence of orthogonal polynomials $\{p_k(x)\}_{k=1}^m$ w.r.t. measure μ , that is: $\int_{\lambda_d}^{\lambda_1} p_n(x)p_m(x)d\mu(x) = \delta_{m,n}$, where $\delta_{m,n} = 1$ if $m = n$ and $\delta_{m,n} = 0$, otherwise. Assume $f(x)$ is a polynomial with degree $< 2m$, then there exists $\{(c_j, x_j)\}_{j=1}^m$ s.t. $\int_{\lambda_d}^{\lambda_1} f(\lambda)d\mu(\lambda) = \sum_{i=1}^m c_j f(x_j)$. The equality holds when x_j are the roots of $p_m(x)$ and $c_j = \int_{\lambda_d}^{\lambda_1} \prod_{j \neq i} \frac{x-x_i}{x_j-x_i} d\mu$. Such choice of $\{(c_j, x_j)\}_{j=1}^m$ are called the Gaussian Quadrature rules.

Theorem 3 shows the existence of good $\{(c_j, x_j)\}_{j=1}^m$ and their general form. In fact, it is also shown that Gaussian Quadrature is optimal: no other $\{(c_j, x_j)\}_{j=1}^m$ can achieve zero approximation error for higher degree polynomials $f(\lambda)$ [Golub and Meurant, 2009]. However, it is often difficult to find these quadrature rules [Golub and Welsch, 1969]. There are at least three questions in sequel:

- 1) how to find the orthogonal polynomials $\{p_k(x)\}_{k=1}^m$ w.r.t. an unknown measure μ ?
- 2) how to efficiently find the roots of $p_m(x)$, which gives the nodes x_j ?
- 3) how to efficiently calculate the weights $c_j = \int_{\lambda_d}^{\lambda_1} \prod_{j \neq i} \frac{x-x_i}{x_j-x_i} d\mu$?

We first answer question 2) and 3) and leave question 1) for later discussion.

Now suppose that we have found the orthogonal polynomials $\{p_k(x)\}_{k=1}^m$ w.r.t. μ . Recall that any orthogonal polynomial has the following "three-term" recursion [Golub and Meurant, 2009]:

$$p_{k+1}(x) = (x - \alpha_{k+1}) p_k(x) - \beta_k p_{k-1}(x), k = 0, 1, \dots,$$

where $p_{-1}(x) \equiv 0, p_0(x) \equiv 1, \alpha_{k+1} = \frac{\langle x p_k, p_k \rangle}{\langle p_k, p_k \rangle}$ and $\beta_k = \frac{\langle p_k, p_k \rangle}{\langle p_{k-1}, p_{k-1} \rangle}$. Define $P_m(x) = (p_0(x), p_1(x), \dots, p_{m-1}(x))^T \in \mathbb{R}^m$, we can rewrite the recursion formula in matrix form (given x): $xP_m = J_m P_m + \beta_m p_m(x) e^m$, where e^m is the last column of identity matrix $I_{m,m}$ and J_m is called Jacobi matrix of order m :

$$J_m = \begin{pmatrix} \alpha_1 & \sqrt{\beta_1} & & & \\ \sqrt{\beta_1} & \alpha_2 & & & \\ & \sqrt{\beta_2} & \alpha_3 & & \\ & & \ddots & \ddots & \ddots \\ & & & & \alpha_m \end{pmatrix} \in \mathbb{R}^{m \times m}$$

It turns out that J_m can help us find the Gaussian Quadrature rules $\{(c_j, x_j)\}_{j=1}^m$ and thus provide answers for question 2) and 3). This is shown in the following theorem.

Theorem 4. [Golub and Meurant, 2009] For the Gaussian Quadrature, $\{x_j\}_{j=1}^m$ are the eigenvalues of J_m and $\{c_j\}_{j=1}^m$ are the squares of the first elements of the normalized eigenvectors of J_m .

The proof of Theorem 4 is based on Christoffel-Darboux relation [Brezinski, 1990]. Now, the remaining question is: how to find the Jacobian matrix J_m of a sequence of orthogonal polynomials w.r.t. an unknown measure μ ? Note that we no longer need to answer question 1) if J_m is found, since J_m is sufficient for us to find the Gaussian quadrature rules. However, it seems impossible to find J_m if no information of μ is provided. The good news is: when the μ is specified as in (8), there exists an efficient way to find J_m .

Step 3. When μ is specified as in (8), J_m can be exactly found in m steps using the Lanczos algorithm [Lanczos, 1950], as shown in Algorithm 4. This method takes a real symmetric matrix as input and returns a tridiagonal matrix. It was originally proposed to solve eigenvalue problems. Later, researchers found a deep connection between the Lanczos algorithm and orthogonal polynomials, which further connects this method to the Gaussian quadrature. The method (of finding the Gaussian quadrature by the Lanczos algorithm) is called the Lanczos quadrature [Golub and Strakoš, 1994, Bai and Golub, 1996, Golub and Meurant, 2009]. An extremely elegant but highly nontrivial result is as follows:

Theorem 5. [Golub and Meurant, 2009] *Given a real symmetric matrix $H \in \mathbb{R}^{d \times d}$ and an arbitrary vector $v \in \mathbb{R}^d$ with unit Euclidean norm, we define the measure μ as in (8) based on this H and v . Then m steps of the Lanczos algorithm return the Jacobian matrix J_m of orthogonal polynomials w.r.t. to μ .*

After J_m is found by the Lanczos algorithm, we perform spectral decomposition of $J_m \in \mathbb{R}^{m \times m}$ to get its eigen-pairs. Using Theorem 4, we successfully get the Gaussian quadrature rules and thus we can approximate the quadratic form $v^T f(H)v$. By averaging over different random vectors v we can then approximate $\frac{1}{d} \text{tr}(f(H))$. This concludes the derivation of SLQ for the trace estimation problem.

The full procedure of SLQ is shown in Algorithm 5. We note that SLQ is efficient in theory. Ubaru et al. [2017] show that SLQ converges faster than any other polynomial expansion method for spectrum estimation (e.g., Chebyshev methods used in [Adams et al., 2018]). See [Ubaru et al., 2017, Theorem 4.1] for a formal statement.

We remark that there are at least four versions of the Lanczos algorithm in **Step 3**. Here, we adopt the version in Algorithm 4 since it is known to be the most numerically stable version [Cullum and Willoughby, 2002, Saad, 2011, Wikipedia, 2023]. Throughout this work, we choose $f(\cdot)$ as the Gaussian blurring function $f(\lambda) := \frac{1}{\sigma\sqrt{2\pi}} \exp\left(-\frac{(t-\lambda)^2}{2\sigma^2}\right)$ for spectrum approximation. We plot the spectrum by sweeping t from the minimal node to the maximal node in Gaussian Quadrature rules.

Algorithm 4 The Lanczos Algorithm

- 1: Input a matrix-vector product $Hv_1 \in \mathbb{R}^d$, where H is a real symmetric matrix and v_1 is an arbitrary vector with Euclidean norm 1. Choose $m \in \mathbb{N}$
 - 2: **Initialization:** Let $w'_1 = Hv_1$, $\alpha_1 = (w'_1)^T v_1$, $w_1 = w'_1 - \alpha_1 v_1$
 - 3: **for** $j = 2 \rightarrow m$ **do**
 - 4: Let $\beta_j = \|w_{j-1}\|_2$ (also Euclidean norm)
 - 5: If $\beta_j \neq 0$, then let $v_j = w_{j-1}/\beta_j$,
 else pick as v_j an arbitrary vector with Euclidean norm 1 that is orthogonal to all of v_1, \dots, v_{j-1}
 - 6: Let $w'_j = Av_j$
 - 7: Let $\alpha_j = (w'_j)^T v_j$
 - 8: Let $w_j = w'_j - \alpha_j v_j - \beta_j v_{j-1}$
 - 9: **end for**
 - 10: Let V be the matrix with columns v_1, \dots, v_m
 - 11: Let $T = \begin{pmatrix} \alpha_1 & \beta_2 & & & & 0 \\ \beta_2 & \alpha_2 & \beta_3 & & & \\ & \beta_3 & \alpha_3 & \ddots & & \\ & & \ddots & \ddots & \beta_{m-1} & \\ & & & \beta_{m-1} & \alpha_{m-1} & \beta_m \\ 0 & & & & \beta_m & \alpha_m \end{pmatrix}$
 - 12: Return T
-

Algorithm 5 The Stochastic Lanczos Quadrature Method

- 1: Choose $\text{num}_v, m \in \mathbb{N}$. Sample num_v i.i.d. v_i from normalized Rademacher distribution, $i \in [\text{num}_v]$
 - 2: **for** $i = 1 \rightarrow \text{num}_v$ **do**
 - 3: Run m steps of the Lanczos Algorithm 4 with input Hv_i , returns $T \in \mathbb{R}^{m \times m}$
 - 4: Compute eigenvalue decomposition $T = Q\Lambda Q^T$
 - 5: Compute the nodes $x_i = (\Lambda_{ii})_{i=1}^m$ and weights $c_i = \left(Q_{1,i}^2\right)_{i=1}^m$
 - 6: Return $q_i(t) = \sum_{i=1}^m c_i f(x_i; t, \sigma^2)$
 - 7: **end for**
 - 8: Return $\frac{1}{\text{num}_v} \sum_{i=1}^{\text{num}_v} f(\ell_i; t, \sigma^2)$
-

C More Experimental Details

C.1 Implementation Details on SLQ

Implementation and Running Time Analysis. We provide a simple PyTorch implementation of SLQ. The only query SLQ makes to the neural network is the Hessian vector product, which is attained using the auto-differentiation framework [Pearlmutter, 1994]. To assure the accuracy of the Lanczos algorithm, we remove all the randomness in the forward and backward passes, including: data shuffling order, data augmentation, and dropout, etc.. Since Flash Attention [Dao et al., 2022] does not support the calculation of Hessian-vector product, we implement all attention blocks in the naive way. For the calculation of the blockwise Hessian spectrum $\nabla^2 \mathcal{L}(w_l)$, we sample $u_l \sim N(0, I_{d_l \times d_l})$ and set $v_l = u_l / \|u_l\|_2 \in \mathbb{R}^{d_l}$. Then we run Algorithm 5 by taking $\nabla^2 \mathcal{L}(w_l)$ and v_l as inputs. We choose the hyperparameters as $m = 100$ and $n_v = 10$ in all experiments. σ is tuned based on visual effects. These hyperparameters are reported to reach highly accurate estimation with error $< 10^{-14}$ [Ghorbani et al., 2019].

We now briefly discuss the computational cost of SLQ. The major computational expense of SLQ is the repeated Hessian-vector product operations in Lanczos algorithm in **Step 3**. Recall $\nabla^2 \mathcal{L}(w)d = \frac{1}{n} \sum_{i=1}^n \nabla^2 \mathcal{L}_i(w)d$, so each Hessian-vector product operation requires (i) calculating $\nabla^2 \mathcal{L}_i(w)d$; (ii) repeating (i) on all data. We point out that (i) can be computed efficiently and precisely with just two backpropagation passes [Pearlmutter, 1994]. The major computational bottleneck lies in (ii) due to the large n . Our largest-scale experiment for Hessian spectrum is GPT2 (125M) on Openwebtext, where the number of tokens $n = 9$ Billion. To calculate $\nabla^2 \mathcal{L}(w)d$ on all these 9B tokens, it requires about 9 GPU days on eight A100-80GB GPUs. Since SLQ requires at least 1,000 times query of $\nabla^2 \mathcal{L}(w)d$, a complete run of SLQ would take at least 9,000 days on eight A100-80GB GPUs, which is unaffordable. In this work, we use the largest possible batch size (with gradient accumulation tricks) to approximate $\nabla^2 \mathcal{L}(w)$ under the constraints of GPU bandwidth and time limit. More detailed setup of SLQ are shown as follows.

- **ResNet18 (20M) and VGG16 (138M) on ImageNet.** We use the code base of PyTorch Examples ⁴. We use batch size = 1024. For the calculation of the blockwise Hessian spectra, we apply SLQ to all parameter blocks except for the BatchNorm layers. In total, it takes about 3 days on one V100 GPU to estimate all the blockwise Hessian spectra and the full Hessian spectrum.
- **ViT-base (86M) on ImageNet.** We use the code base of PyTorch Image Models ⁵. We use batch size = 1024. Due to the large number of parameters, we are not able to calculate the blockwise Hessian spectra for all parameter blocks. Instead, we apply SLQ to: the embedding layer; the output layer; the 1-st, 6-th, 12-th attention blocks; and the 1-st, 6-th, 12-th MLP blocks (note that the 12-th attention and MLP blocks are the final ones). In total, it takes about 3 days on one V100 GPU to estimate all the blockwise Hessian spectra and the full Hessian spectrum.

⁴<https://github.com/pytorch/examples/blob/main/imagenet/main.py>

⁵<https://github.com/huggingface/pytorch-image-models>

- **BERT(40M) on Cornell Movie-Dialogs Corpus.** We use the code base from the blog⁶. We use batch size = 327,680 tokens. For the calculation of the blockwise Hessian spectra, we apply SLQ to all parameter blocks except for the LayerNorm layers. In total, it takes about 12 hours on one V100 GPU to estimate all the blockwise Hessian spectra and the full Hessian spectrum.
- **GPT2-nano (11M) on Shakespeare.** We use the code base of NanoGPT⁷. We use batch size = 163,840 tokens. For the calculation of the blockwise Hessian spectra, we apply SLQ to all parameter blocks with even indices, except for the LayerNorm layers. In total, it takes about 12 hours on one V100 GPU to estimate all the blockwise Hessian spectra and the full Hessian spectrum.
- **GPT2 (125M) on Openwebtext.** We use the code base of NanoGPT. We use batch size = 245,760 tokens. Due to the large number of parameters, we are not able to calculate the blockwise Hessian spectra for all parameter blocks. Instead, we apply SLQ to: the embedding layer; the output layer; the 1-st, 4-th, 8-th, 12-th attention blocks; and the 1-st, 4-th, 8-th, 12-th MLP blocks (note that the 12-th attention and MLP blocks are the final ones). In total, it takes about 7 days on one A100 GPU to estimate all the blockwise Hessian spectra and the full Hessian spectrum.

We train all the models under the default configurations in all cases. For CNN training, we follow the rule of thumb to choose the learning rate of AdamW: we set the learning rate of AdamW to be $100\times$ smaller than the recommended learning rate of SGD.

C.2 Implementation Details on Figure 2

We use the code base of NanoGPT to train a decoder-only Transformers on 4 consecutive tokens randomly selected from Openwebtext. We set the model configuration as: context window = 2, number of heads = 2 and the embedding dimension = 4. In MLP layers, all widths equal to 4. We change the number of layers from 1 to 4. We remove all the Layer Norms in the model. The rest of the model configurations are set to their default values in the code base. We compute the Hessian on all the parameters blocks in attention and MLP layers. In Figure 2 (a), the variables in three blue boxes corresponds to the parameters in Query and Key; Value and Projection; and MLP, respectively. Similarly for the rest of the figures.

Due to the intensive overhead of computing and storing the whole Hessian, we have yet to check the block-diagonal structure on larger models. Rigorously speaking, so far we have not gotten sufficient evidence to claim this structure commonly holds in larger Transformers. It requires new numerical methods to efficiently check the block-diagonal Hessian structure in larger models without explicitly calculating them. We leave it as an interesting future direction.

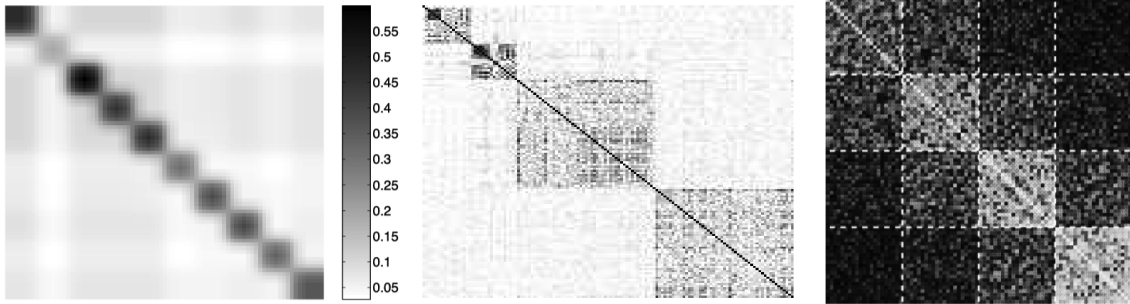
For completeness, we remark that Collobert [2004], Roux et al. [2007], Martens and Grosse [2015] also observed the block-diagonal structure in (approximated) Hessian of small-scaled MLPs. We restate their findings in Figure 9. [Collobert, 2004, Section 7] further theoretically proved that the block diagonal structure stems from (i) the layer-by-layer structure and (ii) the Cross-Entropy loss. These results suggest that block-diagonal structure might be common in NNs.

C.3 Implementation Details on the MLP experiments in Figure 5

We train a 4-layer MLP on MNIST. We use batch size = 128 and width = 300, 128, and 64 for the hidden layers. We use ReLU activation. We change the degree of heterogeneity by scaling the output of each layer with constant $c \in \mathbb{N}$. We scale c from 1 to 15. We record the average JS distance between the initial Hessian spectra of each pair of layers and find that the average JS distance increases as c increases. As such, we define c as the degree of block heterogeneity. For each c , we train SGD and Adam with default hyperparameters by grid-searching the learning rate from $1e-4$ to $1e-1$ and report the best test accuracy after 1 epoch.

⁶<https://medium.com/data-and-beyond/complete-guide-to-building-bert-model-from-scratch-3e6562228891>

⁷<https://github.com/karpathy/nanoGPT/>



(a) Trained Hessian of a MLP in [Collobert, 2004], Figure 7.4 (b) Approximated trained Hessian of a MLP in [Roux et al., 2007], Figure 1 (c) Approximated trained Hessian of a MLP in [Martens and Grosse, 2015], Figure 6

Figure 9: The block-diagonal structure in the (approximated) Hessian of MLPs reported in the literature.

c	1	2	3	4	5	6	7	8	9-15
Blockwise distance	1e-3	1.61	33.99	65.32	260.77	298.39	351.69	353.48	NaN

Table 3: Consider a 4-layer MLP on MNIST. c denotes the scaler that is multiplied to the output of each layer. Blockwise distance denotes the average JS distance between the initial Hessian spectra of each pair of layers. We find that the average JS distance increases as c increases. For $c \geq 9$, the calculation of JS distance encounters numerical instability due to the division of near-zero values and returns NaN.

D More Experimental Results

D.1 Performance comparison of AdamW and SGD on Different Architectures

Here, we show the performance comparison of AdamW and SGD on different models.

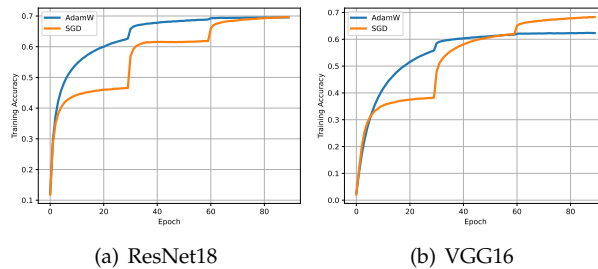


Figure 10: Performance of AdamW and SGD on CNNs including ResNet18 and VGG16. SGD and Adam perform similarly on these tasks.

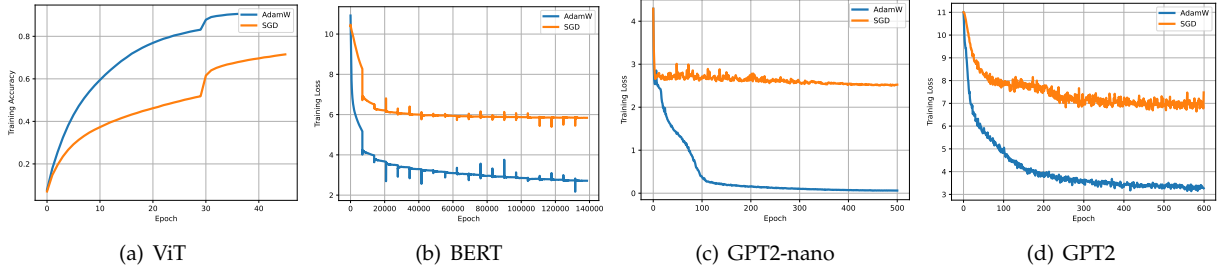


Figure 11: Performance of AdamW and SGD on Transformers including ViT, BERT, GPT2-nano, and GPT2. SGD performs significantly worse than Adam on these tasks.

E Proofs

E.1 Proof of Proof of Proposition 1

Let $H = \begin{bmatrix} L & 0 \\ 0 & \mu \end{bmatrix}$, where $L > \mu > 0$. We choose the initial point as $w^0 = (w_1^0, w_2^0) = (\sqrt{\mu/L}, \sqrt{L/\mu})$. By the update rule of GD, we have

$$\begin{aligned}
\mathcal{L}(w^{t+1}) &= \mathcal{L}(w^t - \eta \nabla \mathcal{L}(w^t)) \\
&= \frac{1}{2} (w^t - \eta H w^t)^T H (w^t - \eta H w^t) \\
&= (w_1^t)^2 |1 - \eta L| L + (w_2^t)^2 |1 - \eta \mu| \mu \\
&= |1 - \eta L|^t L \frac{\mu}{L} + |1 - \eta \mu|^t \mu \frac{L}{\mu} \\
&= \mu |1 - \eta L|^t + L |1 - \eta \mu|^t
\end{aligned} \tag{10}$$

To proceed, we discuss the following cases:

When $\eta \leq 1/L$, since $|1 - \eta L|^t$ and $|1 - \eta \mu|^t$ are monotonically decreasing, the optimal solution is $\eta = 1/L$.

When $\eta \geq 1/\mu$, since $|1 - \eta L|^t$ and $|1 - \eta \mu|^t$ are monotonically increasing, the optimal solution is $\eta = 1/\mu$.

When $1/L \leq \eta \leq 1/\mu$, (10) can be written as $g_t(\eta) = \mu(\eta L - 1)^t + L(1 - \eta \mu)^t$. Take the first-order and the second-order derivative of the g , we can obtain $g'_t(\eta) = tL\mu(\eta L - 1)^{t-1} - t\mu L(1 - \eta \mu)^{t-1}$ and $g''_t(\eta) = t(t-1)L^2\mu(\eta L - 1)^{t-2} + t(t-1)\mu^2(1 - \eta \mu)$. Since $g''_t(\eta) \geq 0$ for all $\eta \in [1/L, 1/\mu]$, the function g is convex. By solving the equation that $g'_t(\eta) = 0$, we can obtain $\eta = \frac{2}{L+\mu}$ is a solution for all t . Plugging this result into (10) and rearranging the terms, we conclude the proof of Proposition 1.

E.2 Proof of Theorem 1

Without loss of generality, we assume $h = 0$. This is because minimizing $\mathcal{L}(w) = \frac{1}{2} w^T H w - h^T w$ is equivalent to minimizing $\mathcal{L}(w) = \frac{1}{2} (w - w^*)^T H (w - w^*)$ where $w^* = H^{-1}h$. By a linear transformation $z = w - w^*$, BGD for minimizing $\frac{1}{2} (w - w^*)^T H (w - w^*)$ starting from w^0 is equivalent to BGD for minimizing $\frac{1}{2} z^T H z$ starting from $z^0 = w^0 - w^*$. Thus we can assume $w^* = 0$, or equivalently, $h = 0$. When $h = 0$, the update form of BGD becomes

$$w^{t+1} = w^t - \eta D_{BGD}^{-1} H w^t,$$

where $D_{BGD} = \text{diag} \left(\left(\underbrace{\eta_1, \dots, \eta_1}_{d_1 \text{ times}}, \dots, \underbrace{\eta_L, \dots, \eta_L}_{d_L \text{ times}} \right)^T \right) \in \mathbb{R}^{d \times d}$.

In the following, we will first prove the rate of BGD for each block and then combine them together to get the total rate. For the l -th block, we choose $\eta_l = \frac{1}{\lambda_{l,1}}$. The update rule of BGD for the l -th block becomes:

$$w_l^{t+1} = w_l^t - \frac{1}{\lambda_{l,1}} H_l w_l^t$$

Now we apply the standard convergence proof of GD to the l -th block. By descent lemma, we have

$$[\mathcal{L}(w^{t+1})]_l \leq [\mathcal{L}(w^t)]_l + \langle w_l^{t+1} - w_l^t, [\nabla \mathcal{L}(w^t)]_l \rangle + \frac{\lambda_{l,1}}{2} \|w_l^{t+1} - w_l^t\|_2^2 \quad (11)$$

$$\leq [\mathcal{L}(w^t)]_l + \langle w_l^{t+1} - w_l^t, H_l w_l^t \rangle + \frac{\lambda_{l,1}}{2} \eta^2 w_l^t H_l^T H_l w_l^t \quad (12)$$

$$= [\mathcal{L}(w^t)]_l - \frac{1}{2\lambda_{l,1}} w_l^t H_l^T H_l w_l^t \quad (13)$$

$$\leq [\mathcal{L}(w^t)]_l - \frac{\lambda_{l,d_l}}{2\lambda_{l,1}} w_l^t H_l w_l^t \quad (14)$$

$$= \left(1 - \frac{1}{\kappa_l}\right) [\mathcal{L}(w^t)]_l \quad (15)$$

Subtract both sides by \mathcal{L}^* and we get $[\mathcal{L}(w^{t+1})]_l - [\mathcal{L}^*]_l \leq \left(1 - \frac{1}{\kappa_l}\right) ([\mathcal{L}(w^t)]_l - [\mathcal{L}^*]_l)$. Summing up both sides over $l \in [L]$, we have

$$\begin{aligned} \mathcal{L}(w^{t+1}) - \mathcal{L}^* &= \sum_{l=1}^L ([\mathcal{L}(w^{t+1})]_l - [\mathcal{L}^*]_l) \\ &\leq \sum_{l=1}^L \left(1 - \frac{1}{\kappa_l}\right) ([\mathcal{L}(w^t)]_l - [\mathcal{L}^*]_l) \\ &\leq \max_{l \in [L]} \left(1 - \frac{1}{\kappa_l}\right) \sum_{l=1}^L ([\mathcal{L}(w^t)]_l - [\mathcal{L}^*]_l) \\ &= \max_{l \in [L]} \left(1 - \frac{1}{\kappa_l}\right) (\mathcal{L}(w^t) - \mathcal{L}^*). \end{aligned}$$

This concludes the proof of Theorem 1.

E.3 Proof of Theorem 2

Similarly as the proof of Theorem 1, we assume $h = 0$. The update rule of Adam becomes

$$w^{t+1} = w^t - \eta (D_{Adam}^0)^{-1} H w^t,$$

where $D_{Adam}^0 = \text{diag}(\nabla \mathcal{L}(w^0) \circ \nabla \mathcal{L}(w^0))^{\frac{1}{2}} = \text{diag}(|H w^0|)$. We denote $d_t = \eta (D_{Adam}^0)^{-1} H w^t$ and thus we have $w^t = \frac{1}{\eta} H^{-1} D_{Adam}^0 d^t$ and $w^{t+1} = w^t - d_t$. These relations also hold for each block by changing the notation to $H_l w_l^t$, D_{Adam}^0 , and d_l^t , etc.. Following the framework in [Sun and Ye, 2021], we try to bound the error yet to be optimized (a.k.a., cost-to-go) and the per-step improvement, respectively. The ratio of these two terms characterizes the rate of convergence. We now express both terms using d_l^t . For the cost-to-go term for the l -th block, we have

$$[\mathcal{L}(w^t)]_l - [\mathcal{L}^*]_l = \frac{1}{2}(w_l^t)^T H_l w_l^t = \frac{1}{2\eta^2}(d_l^t)^T D_{Adam,l}^0 H_l^{-1} D_{Adam,l}^0 d_l^t. \quad (16)$$

For the per-step improvement, we have

$$\begin{aligned} [\mathcal{L}(w^t)]_l - [\mathcal{L}(w^{t+1})]_l &= \frac{1}{2}(w_l^t)^T H_l w_l^t - \frac{1}{2}(w_l^{t+1})^T H_l w_l^{t+1} \\ &= \frac{1}{2}(w_l^t)^T H_l w_l^{t+1} - \frac{1}{2}(w_l^t - d_l^t)^T H_l (w_l^t - d_l^t) \\ &= (d_l^t)^T H_l w_l^t - \frac{1}{2}(d_l^t)^T H_l d_l^t \\ &= \frac{1}{2}(d_l^t)^T \left(\frac{2}{\eta} D_{Adam,l}^0 - H_l \right) d_l^t. \end{aligned} \quad (17)$$

To proceed, we denote $\hat{H} = (D_{Adam}^0)^{-1}H$ and we denote its eigenvalues as $\hat{\lambda}_1 \geq \hat{\lambda}_2 \geq \dots \hat{\lambda}_d$. Similarly, we denote $\hat{H}_l = (D_{Adam,l}^0)^{-1}H_l$ and its eigenvalues $\hat{\lambda}_{l,1} \geq \hat{\lambda}_{l,2} \geq \dots \hat{\lambda}_{l,d_l}$. Let $\eta = \min_{l \in [L]} C_{l,1}$, we have

$$\begin{aligned} \frac{[\mathcal{L}(w^t)]_l - [\mathcal{L}^*]_l}{[\mathcal{L}(w^t)]_l - [\mathcal{L}(w^{t+1})]_l} &= \frac{\frac{1}{\eta^2}(d_l^t)^T D_{Adam,l}^0 H_l^{-1} D_{Adam,l}^0 d_l^t}{(d_l^t)^T \left(\frac{2}{\eta} D_{Adam,l}^0 - H_l \right) d_l^t} \\ &\leq \left\| \frac{1}{\eta^2} \left(\frac{2}{\eta} D_{Adam,l}^0 - H_l \right)^{-1} D_{Adam,l}^0 H_l^{-1} D_{Adam,l}^0 \right\|_2 \end{aligned} \quad (18)$$

$$\stackrel{(*)}{\leq} \frac{C_{l,2}^2 \lambda_{l,1}^2}{(\min_{l \in [L]} C_{l,1}^2) \lambda_{l,1} \lambda_{l,d_l}} \quad (19)$$

$$\leq \left(\max_{l \in [L]} \frac{C_{l,2}^2}{C_{l,1}^2} \right) \kappa_l, \quad (20)$$

where $(*)$ is due to: by Assumption 1, $D_{Adam,l}^0 \preccurlyeq C_{l,2} \lambda_{l,1} I$, $\frac{2}{\eta} D_{Adam,l}^0 - H_l \succcurlyeq \left(\frac{2}{C_{l,1}} C_{l,1} \lambda_{l,1} - \lambda_{l,1} \right) I \succcurlyeq \lambda_{l,1} I$, where \preccurlyeq and \succcurlyeq are matrix inequalities. By rearranging both sides of (20), we have $[\mathcal{L}(w^{t+1})]_l - [\mathcal{L}^*]_l \leq \left(1 - \frac{1}{\left(\max_{l \in [L]} \frac{C_{l,2}^2}{C_{l,1}^2} \right) \kappa_l} \right) ([\mathcal{L}(w^t)]_l - [\mathcal{L}^*]_l)$. Summing up both sides over $l \in [L]$ and we conclude the proof.

$$\begin{aligned} \mathcal{L}(w^{t+1}) - \mathcal{L}^* &= \sum_{l=1}^L ([\mathcal{L}(w^{t+1})]_l - [\mathcal{L}^*]_l) \\ &\leq \sum_{l=1}^L \left(1 - \frac{1}{\left(\max_{l \in [L]} \frac{C_{l,2}^2}{C_{l,1}^2} \right) \kappa_l} \right) ([\mathcal{L}(w^t)]_l - [\mathcal{L}^*]_l) \\ &\leq \max_{l \in [L]} \left(1 - \frac{1}{\left(\max_{l \in [L]} \frac{C_{l,2}^2}{C_{l,1}^2} \right) \kappa_l} \right) \sum_{l=1}^L ([\mathcal{L}(w^t)]_l - [\mathcal{L}^*]_l) \\ &= \max_{l \in [L]} \left(1 - \frac{1}{\left(\max_{l \in [L]} \frac{C_{l,2}^2}{C_{l,1}^2} \right) \kappa_l} \right) (\mathcal{L}(w^t) - \mathcal{L}^*). \end{aligned}$$